Gulf of Mexico Hydrate Mapping and Interpretation Analysis

Phase-II, Project Area 2.4 Report

Aditya Kumar, Alexey Portnov and Ann Cook

October 31, 2022

This report satisfies Mapping and Prospect Identification within Area 4 for BOEM award Gulf of Mexico Gas Hydrate Mapping and Interpretation Analysis, which is Deliverable/Milestone 2.

Table of Contents

Table 1. List of required deliverables and figures.

Sr.	Deliverable	Figure #
1	A map showing the spatial distribution of BSRs within Project Area 2.4	2
2	Regional seismic cross sections showing the base of gas hydrate stability and the relationship of prospective reservoir intervals to channel levee systems, faults, salt, and other geologic features	9-12, 14, 16-18, 21,22,24-26, 28-31,33-35, 37, 38
3	Maps showing the distribution of shallow turbidite channel levee systems	15, 20, 27, 36
4	Average amplitude maps showing the prospective reservoirs based on direct seismic indicators (peak-leading reflections).	13, 19
5	Subsurface geologic maps of one or more seismic reflectors within the gas hydrate stability zone (or that cross the gas hydrate stability zone) showing the structural environment of the area.	23, 32
6	If wells occur in the vicinity of the prospect, annotated well-logs at each gas hydrate prospect showing the thickness of hydrates within the stability zone, interpreted base of gas hydrate stability, and the presence of free gas beneath the gas hydrate stability zone.	14, 34, 35

1 Study area and data

Project Area 2.4 is located in the Mississippi Canyon (MC) protraction area in the northeastern Gulf of Mexico (Figure 1a, b). The water depths range between 150-2400 meters (Figure 1b). The area is characterized by salt mounds, ridges, landslides and canyon systems. BOEM previously identified several BSR zones in this area (Shedd et al., 2012) (Figure 2). Thermogenic hydrate was also recovered in piston cores from MC-945 (Milkov & Sassen, 2001). We identify eight new BSR systems in Project Area 2.4 that were previously not identified by BOEM (Figure 2).

Interestingly, all the identified BSR zones in Project Area 2.4 spatially coincide with landslides or salt bodies. The shallowest BSR is observed at a water depth of 800 meters in Zone-1(Figure 2) and it underlies a landslide scarp. This landslide, the Chandeleur Landslide, was described by Martinez et al. (2022) and covers an area of ~1000 km^2 and contains ~300 km^3 of sediment. Most of the BSRs identified above the salt bodies are clustered BSRs (Portnov et al., 2019) and are associated with the fault systems induced by salt tectonics. Several paleochannel systems are identified near and within the BSRs and may indicate coarse-grained reservoirs for high saturation gas hydrate deposits. Coarse-grained sediment is defined herein as sand or coarse-silt deposits.

Within Project Area 2.4, we use ten seismic surveys in the NAMSS database (Figure 1, Table 1). The total area of Project Area 2.4 is 8250 km^2 and it has full-3D seismic data coverage.

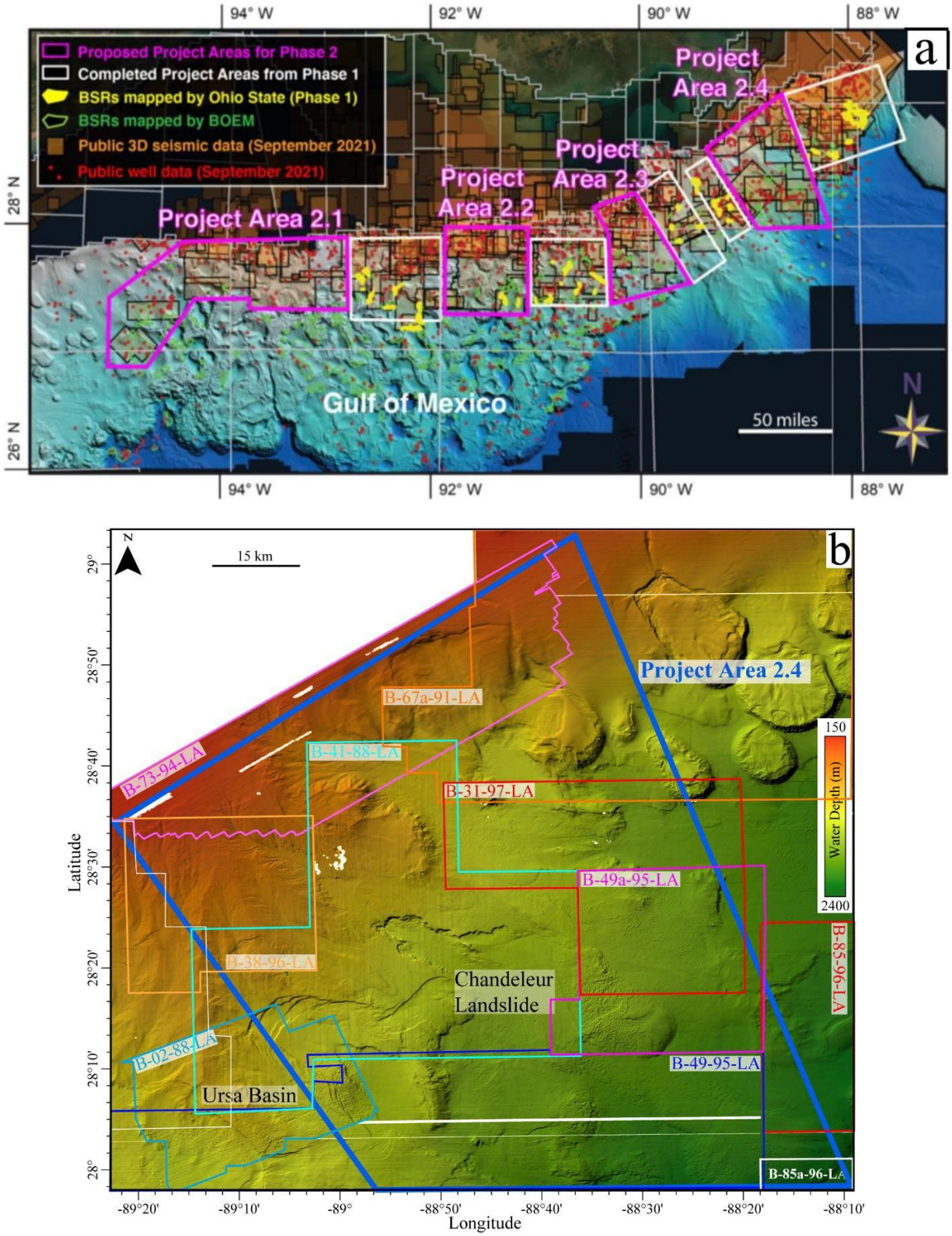

Figure 1: a) A bathymetry map of the northern Gulf of Mexico showing Project Areas of Phase 1 (white squares) and Phase 2 (Pink squares). b) Outlines of the seismic surveys used in this study are rendered over the seafloor bathymetry map. The seafloor bathymetry is mapped in this study using seismic data. The thick blue box shows the outline of Project Area 2.4

Survey number	Survey name/BOEM identifier	Year	Area of seismic survey (km^2)	Frequency Range (Hz)	Survey quality	Bin size (m)	Projection
1	B-38-96-LA/L96-038	1996	920	5-75	Good	20×12.5	16N NAD 1927, feet
2	B-31-97-LA/L97-031	1997	780	5-70	Good	20×12.5	16N WGS 1984, meters
3	B-41-88-LA/L88-041	1988	2710	5-70	Poor	26.6×26.6	16N NAD 1927, feet
4	B-49-95-LA/L95-049	1995	2640	5-80	Fair	20×12.5	16N NAD 1927, feet
5	B-49a-95-LA/L95-049	1995	1035	5-80	Fair	20×12.5	16N NAD 1927, feet
6	B-67a-91-LA/L91-067	1991	5030	5-100	Good	26.6×26.6	16N NAD 1927, feet
7	B-73-94-LA/L94-073	1994	1800	5-90	Poor	20×12.5	16N WGS 1984, meters
8	B-85-96-LA/L96-085	1996	1500	7-90	Fair	20×12.5	16N NAD 1927, feet
9	B-85a-96-LA/L96-085	1996	560	7-90	Fair	20×12.5	16N NAD 1927, feet
10	B-02-88-LA/L88-002	1988	840	5-80	Fair	25×10	16N NAD 1927, feet

Table 2: Details on the 3D seismic surveys uploaded for initial data quality analyses within Project Area 2.4. Projected coordinate systems: NAD_1927_BLM_Zone_16N [EPSG,32066], WGS_1984_UTM_Zone_16N [EPSG,32616].

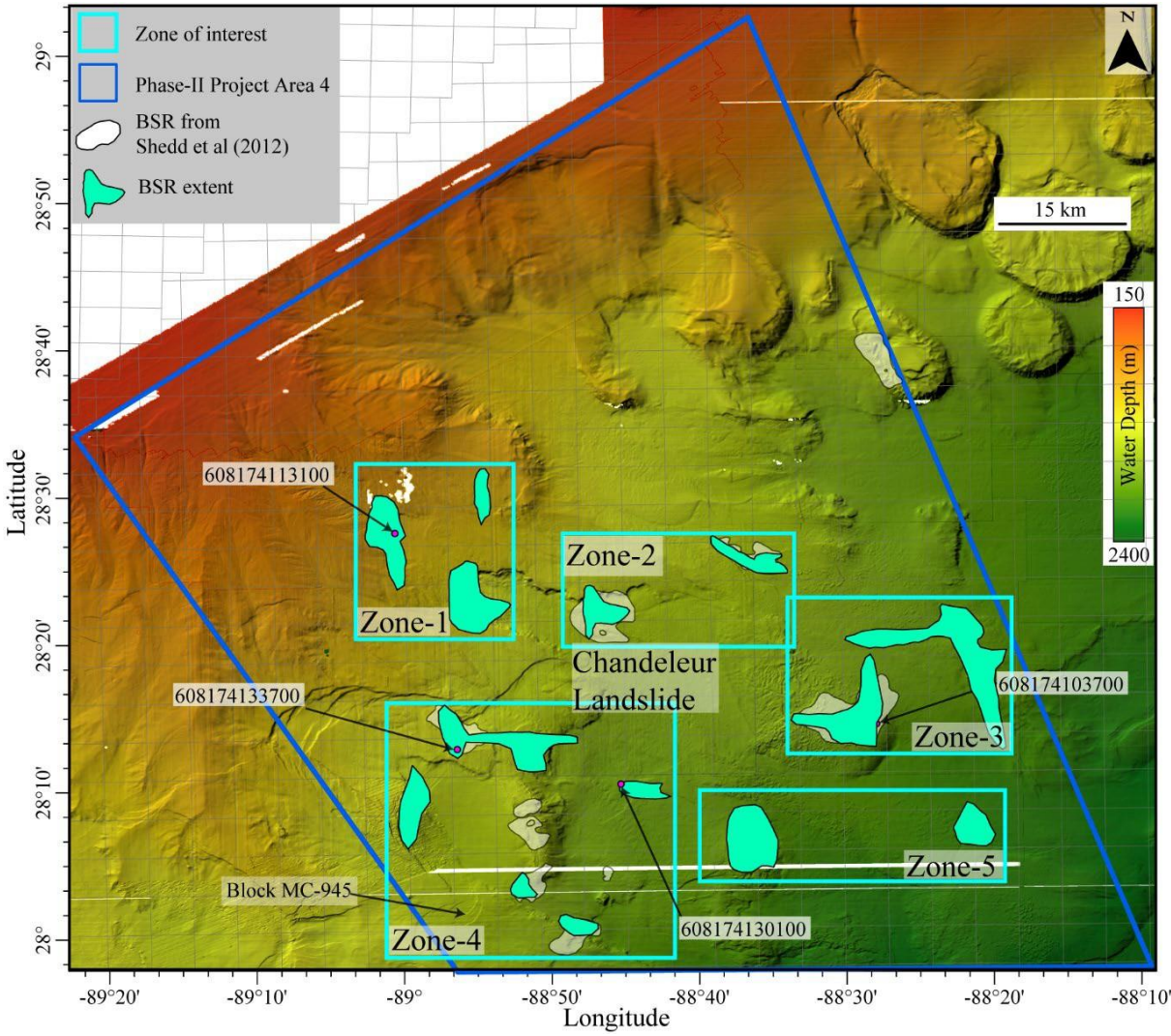

Figure 2: The bathymetry of Project Area 2.4. The large blue polygon is the outline of the Project Area 2.4. The white shapes represent the BSRs previously interpreted by BOEM (Bureau of Ocean Energy Management, 2022). *Light green shapes represent the BSRs interpreted in this project. Interpreted BSRs are grouped into five zones shown by the sky-blue rectangles. Wells used in this study are denoted by the purple dots and labeled with API.*

2 RMS Mapping

To identify BSR-prone areas in Project Area 2.4, regional root-mean-square (RMS) amplitude calculations were performed independently within all 3D seismic surveys (Figure 1a). Because of multiple heat-conductive shallow salt bodies in this area, the geothermal gradient is highly variable, which significantly disturbs the base of the gas hydrate stability zone. Therefore, we extended the depth range of the previous RMS workflow (Project Area 1 Report, Phase 1) to

compute multiple RMS amplitude maps at the following depth intervals (all in msec): 0-50, 50-150, 150-250, 250-350, and 350-450 (Figures 3-7). This allows us to cover all depth intervals and manually inspect all amplitude anomalies in each seismic volume, which allows us to account for the highly variable geothermal gradient.

We group identified BSR systems into five zones (Figure 2, sky blue rectangles). In Project Area 2.4, BSRs are commonly observed within the depth range of 250-450 msec below the seafloor. That is why RMS maps between 250-450 msec intervals (Figures 6 and 7) show good correlation with the mapped BSRs whereas BSR maps of depth intervals between 0-250 msec (Figures 3-5) show very poor correlation. The total area spanned by the BSRs in Project Area 2.4 is ~350 km^2.

RMS amplitude maps were also used to identify paleochannel systems and to identify locations with potentially higher content of course-grained sediments, which we define as sands and coarse silts. Some paleochannels could not be identified with the help of RMS amplitude maps, perhaps due to poor data quality. In addition, the presence of buried mass transport deposits and shallow salt further complicate interpretation of paleochannel systems using RMS amplitude analysis. Therefore, in several areas, paleochannels were tracked manually based on the line-by-line interpretation.

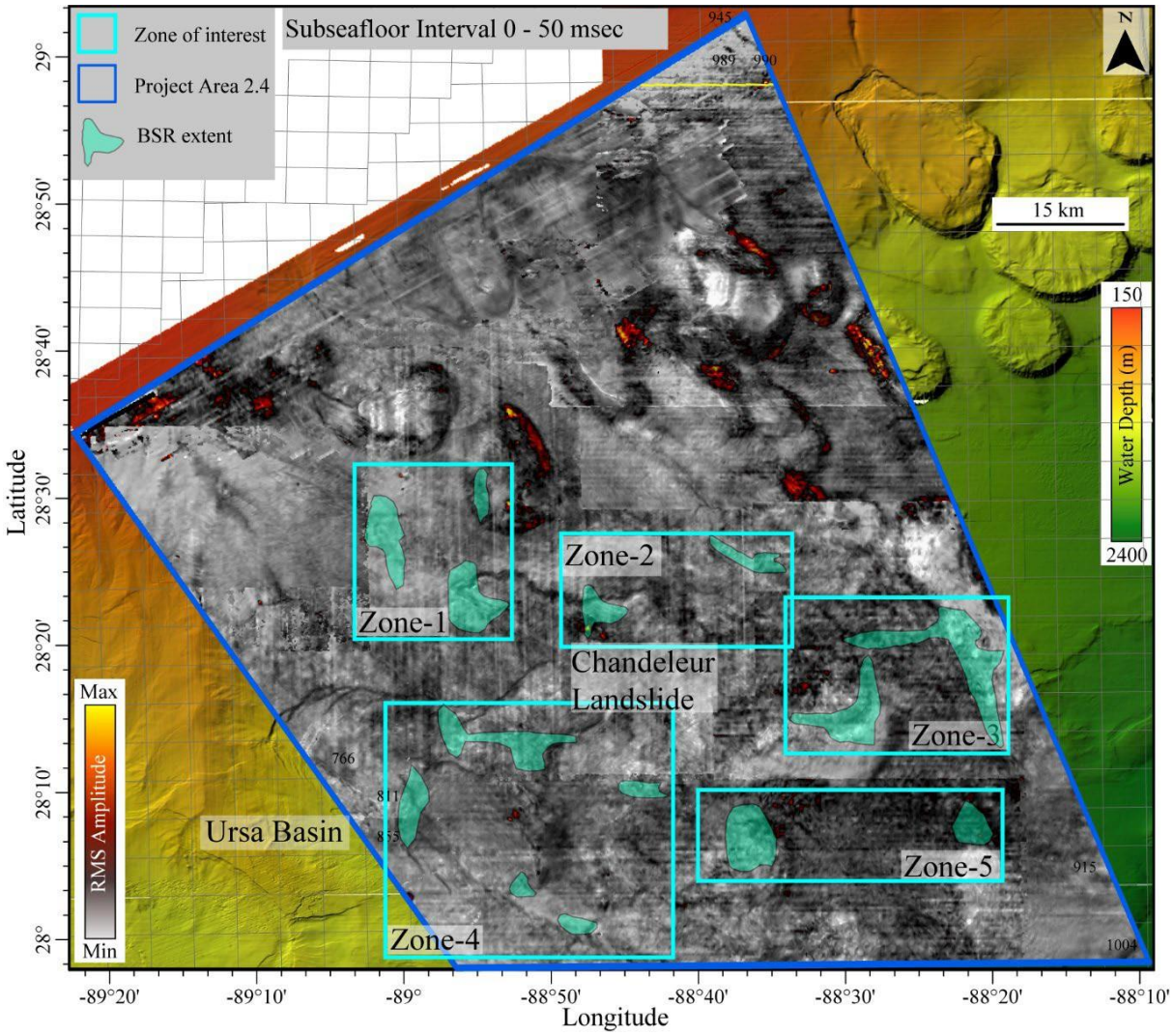

Figure 3: A RMS amplitude map calculated for a subseafloor interval of 0-50 msec.

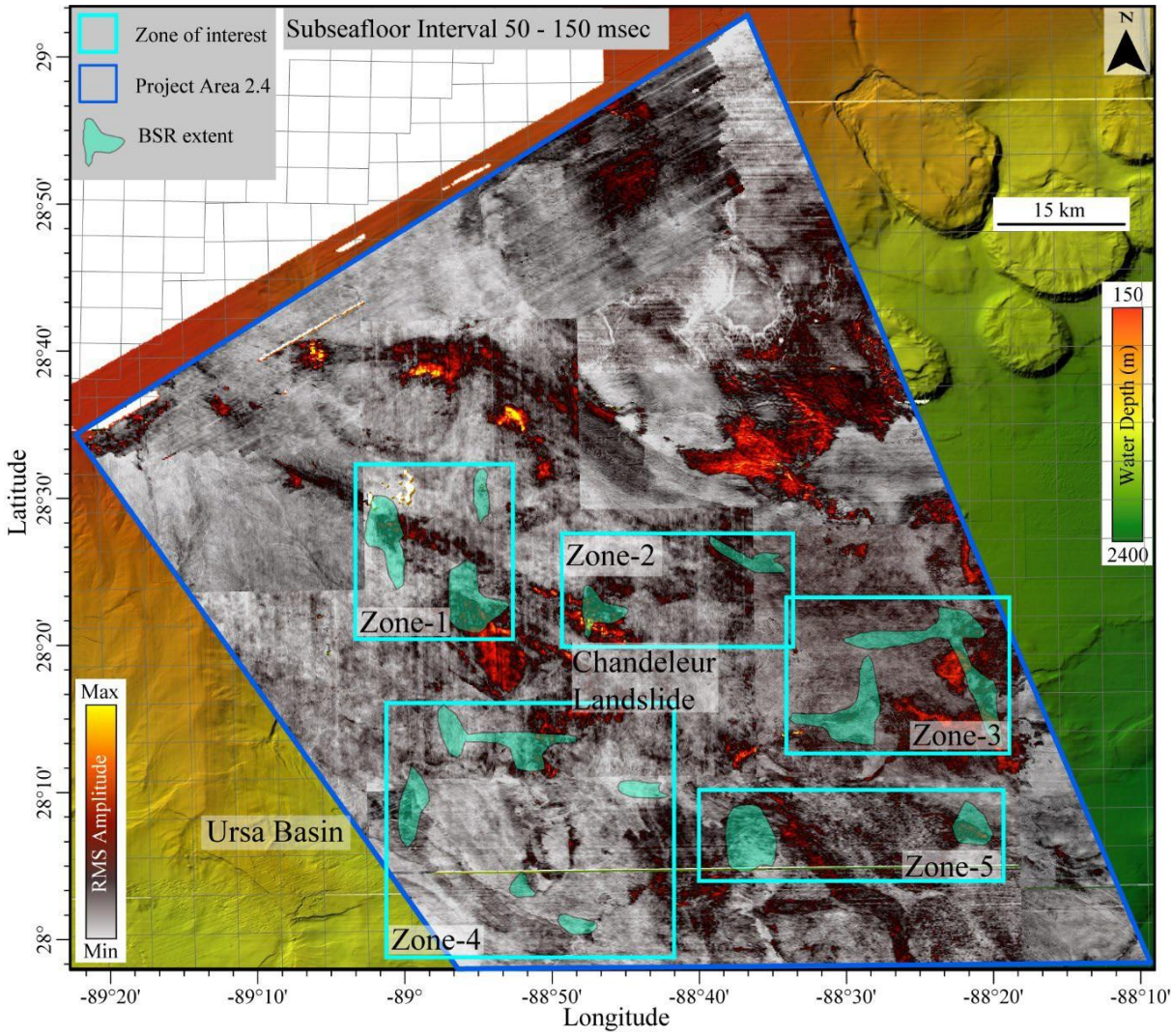

Figure 4: A RMS amplitude map calculated for a subseafloor interval of 50-150 msec.

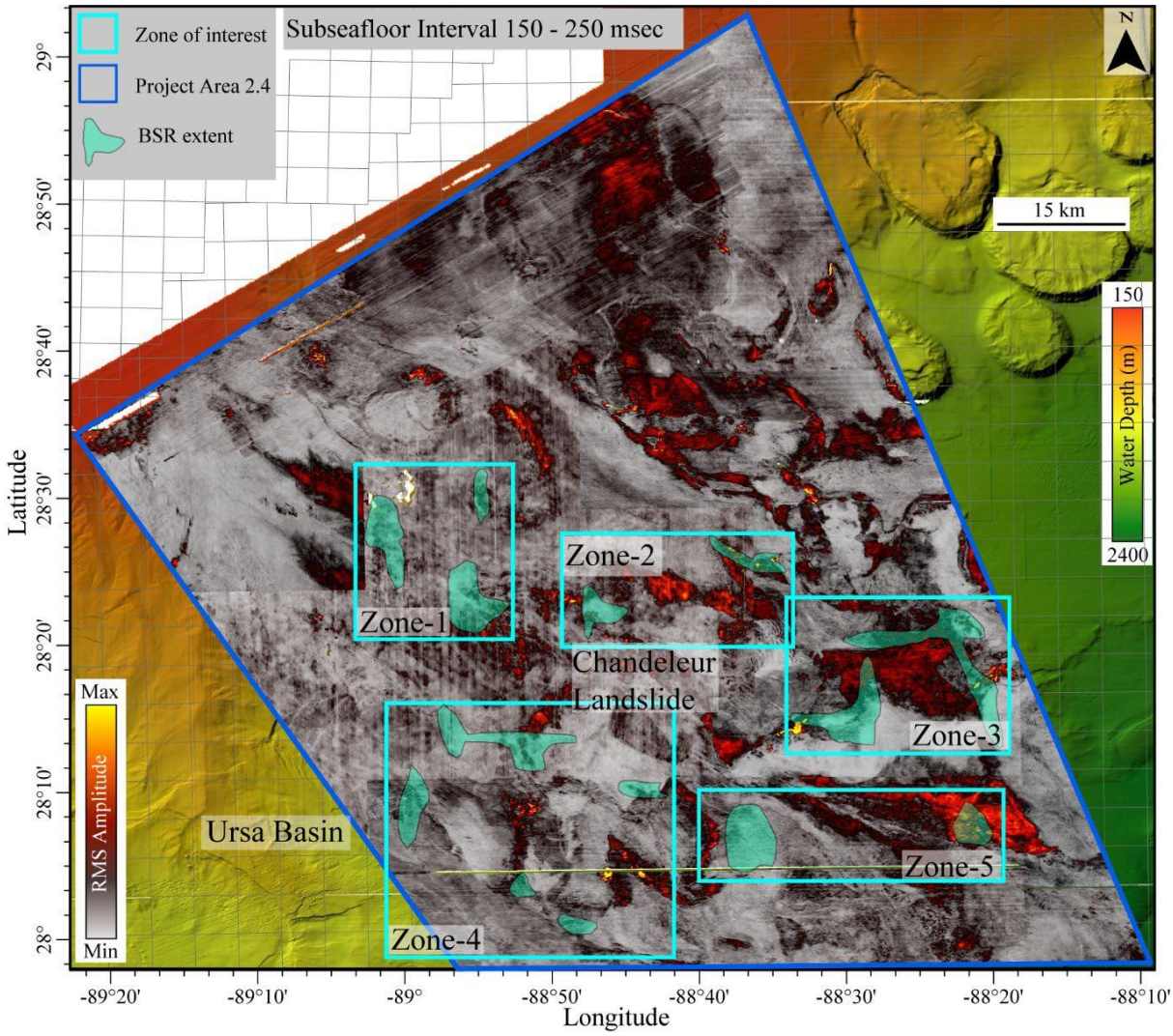

Figure 5: A RMS amplitude map calculated for a subseafloor interval of 150-250 msec.

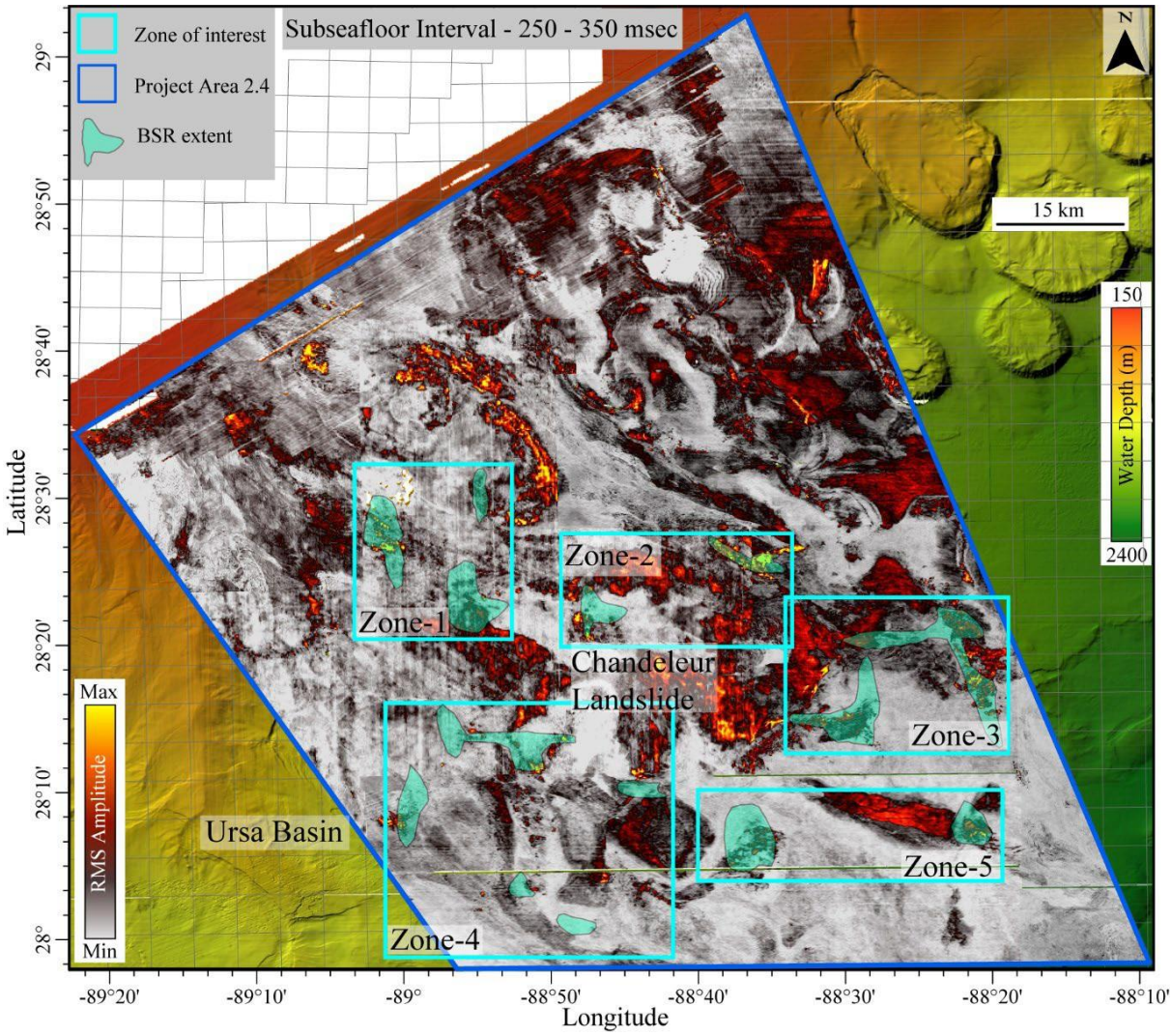

Figure 6: A RMS amplitude map calculated for a subseafloor interval of 250-350 msec.

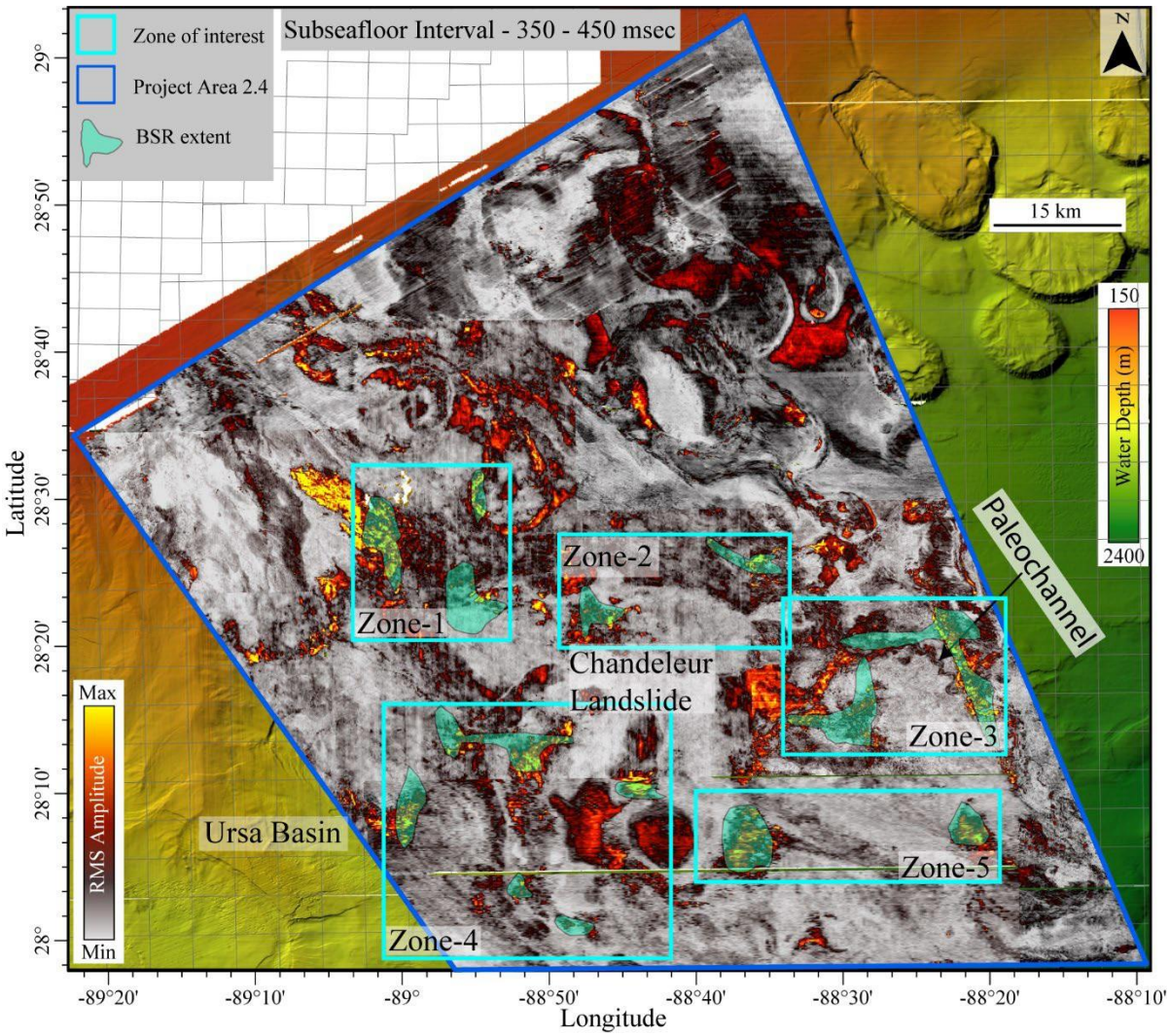

Figure 7: A RMS amplitude map calculated for a subseafloor interval of 350-450 msec.

3 Classification of BSRs

Herein, we classify the BSRs in three different types based on their characteristics in the seismic data: continuous BSRs, discontinuous BSRs, and clustered BSRs. Continuous BSRs are the classic feature, characterized by a continuous, coherent event that crosscuts primary stratigraphy. Unlike the continuous BSR, a discontinuous or segmented BSR is characterized by spaced anomalous seismic events that are generally parallel to seafloor bathymetry. A third type of BSR is clustered BSR, that is characterized as clustered assemblages of high amplitude reflections roughly aligning with the overlying seafloor bathymetry (Portnov et al., 2019). In particular, clustered BSRs occur in the regions of folding or salt diapir rise because these regions host multiple anticlinal and dome

structures that can entrap gas underneath the GHSZ. Such BSRs are common in the Gulf of Mexico and warrant special attention because these BSRs likely indicate high concentrations of gas hydrain turbidite sands (Portnov et al., 2019).

4 Results in Project Area 2.4

4.1 Zone-1:

Zone-1 is located in the northeast of Project Area 2.4 (Figure 2). In water depths of 800-1100 meters, we map three BSR systems that were not previously identified by BOEM (Figure 8). BSRs in the west and southeast region of Zone-1 are located below the head scarps of landslides and span 32 and 36 km^2, respectively (Figure 8). The BSR system in the northeast region is comparatively smaller and covers only a 9 km^2 area. This system is located above a salt diapir (Figure 8, 9). The BSRs are continuous in all three systems (Figure 9, 10, and 11) and are associated with the subsurface fluid flow features, such as seismic chimneys. In some places, landslides disturb the local temperature and pressure conditions, resulting in irregular depth and shape of the BSRs (Figure 12).

BSRs in this zone are present between 350-450 msec TWT (~300 – 400 m) below the seafloor. We estimate the approximate BSR depth in the shallow subsurface using 1700 m/s average sediment velocity. Assuming methane gas composition, the BSR-derived geothermal gradient in this region is between ~30°- 40° C/km (Table 2).

We also observe patches of peak-leading reflections right above the BSR in the western BSR system of Zone-1 (Figure 10). To determine the extent of these peak-leading reflectors average positive amplitudes are calculated within 30 msec window above the BSR. Figure 13 shows a few prominent peak-leading reflection in this system but nothing has been matured into a prospect at this time.

One well (API 608174113100) is drilled within the western BSR system (Figure 8). This well has gamma ray and resistivity measured within the hydrate stability zone. Figure 14 shows the well logs tied to the seismic profile. The seismic-to-well tie is performed using the velocity function provided by Cook and Sawyer (2015) for mud-dominated sediments; mud-rich sediments are the primary lithology in the GHSZ, as shown by the gamma ray log (Figure 14). We observe a small increase in the resistivity (~0.7 ohm.m) just above the estimated depth of the BSR and just below the estimate depth of the BSR. Because the resistivity increase is small, it could be a simple reduction in porosity, a small amount of gas hydrate or a small amount of free gas.

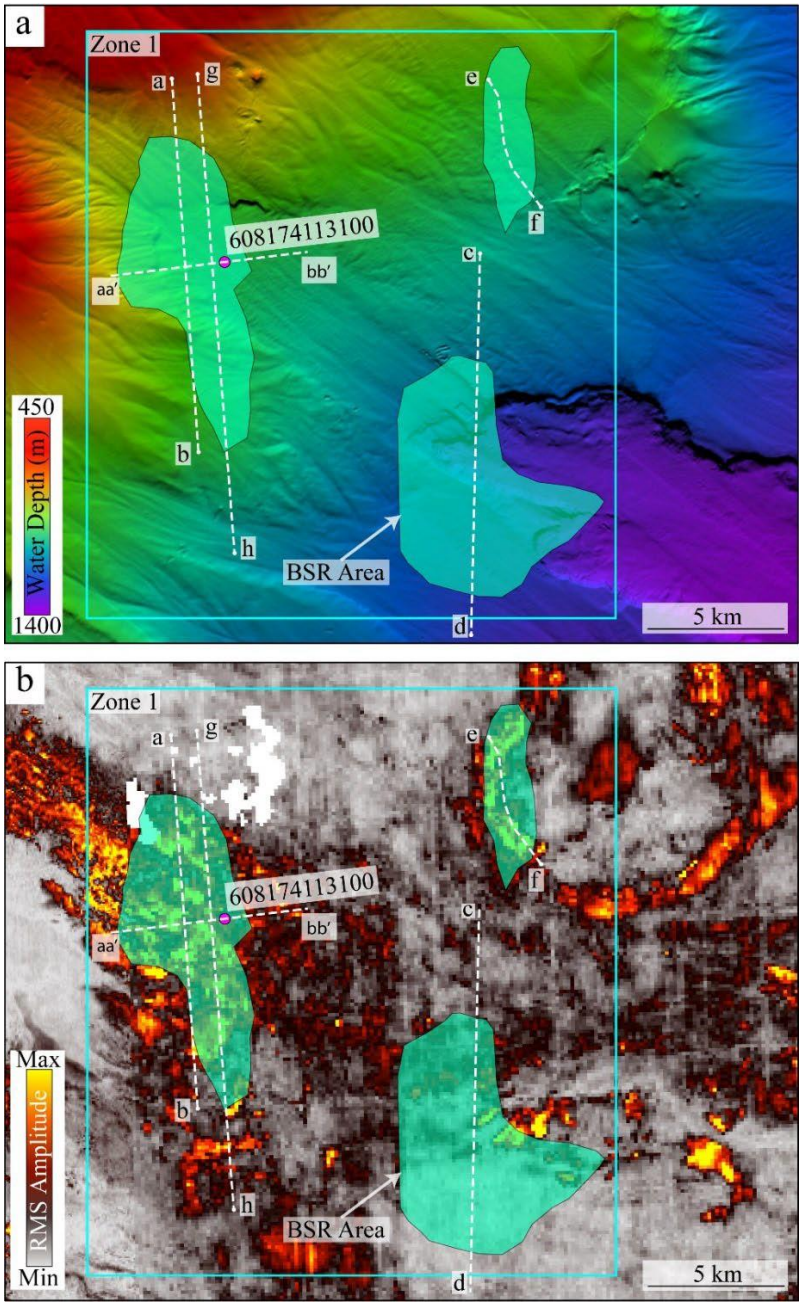

Figure 8: a) A bathymetry map showing the BSR extent and available well log within Project Area 2.4. b) An RMS amplitude map of the sub-seafloor interval between 350-450 msec. White dashed line shows the locations of arbitrary seismic cross-sections shown in the following figures.

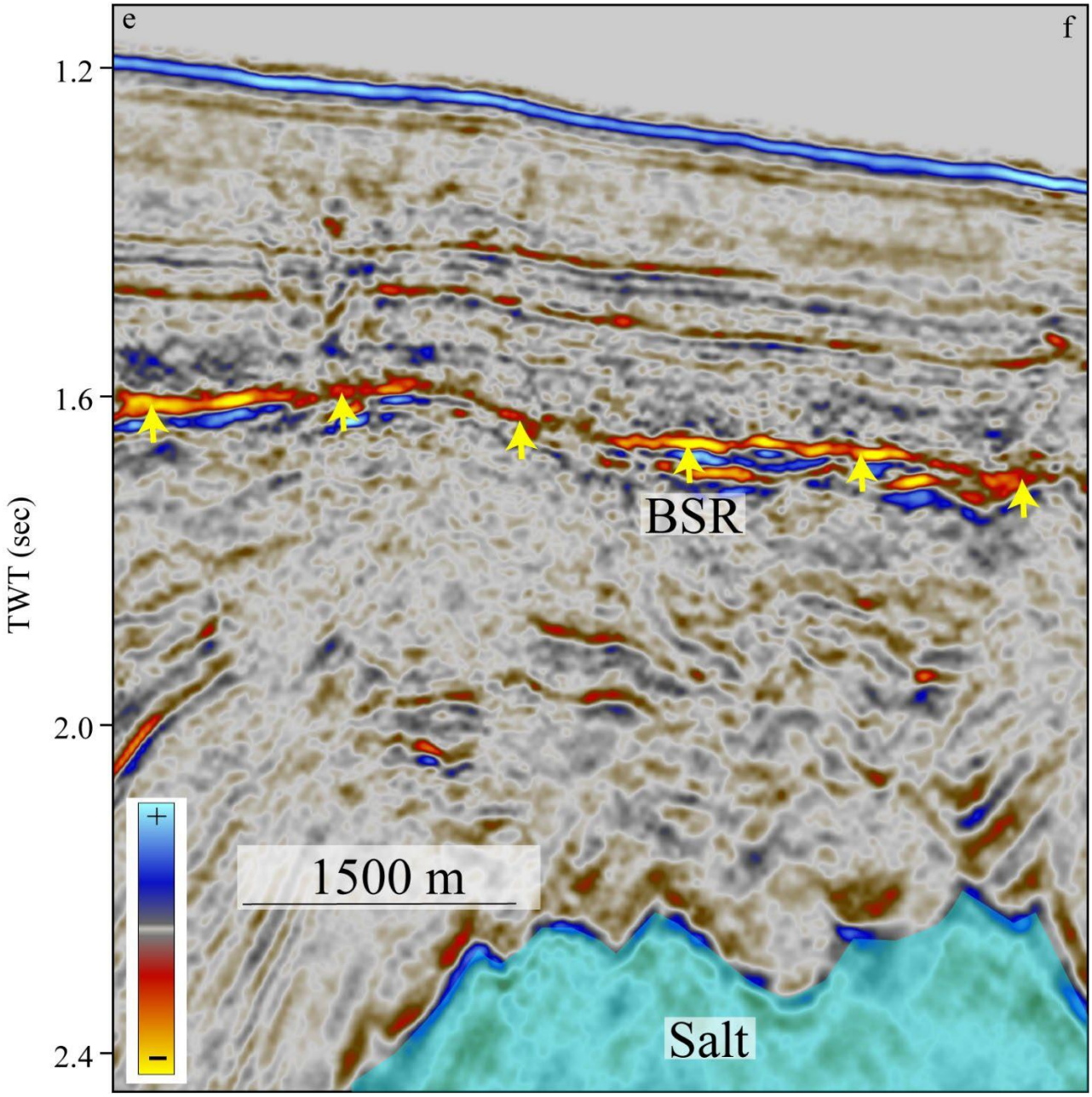

Figure 9: A seismic profile across the northeastern BSR system of Zone-1 showing continuous BSR above the salt diapir. The profile location is shown in Figure 8.

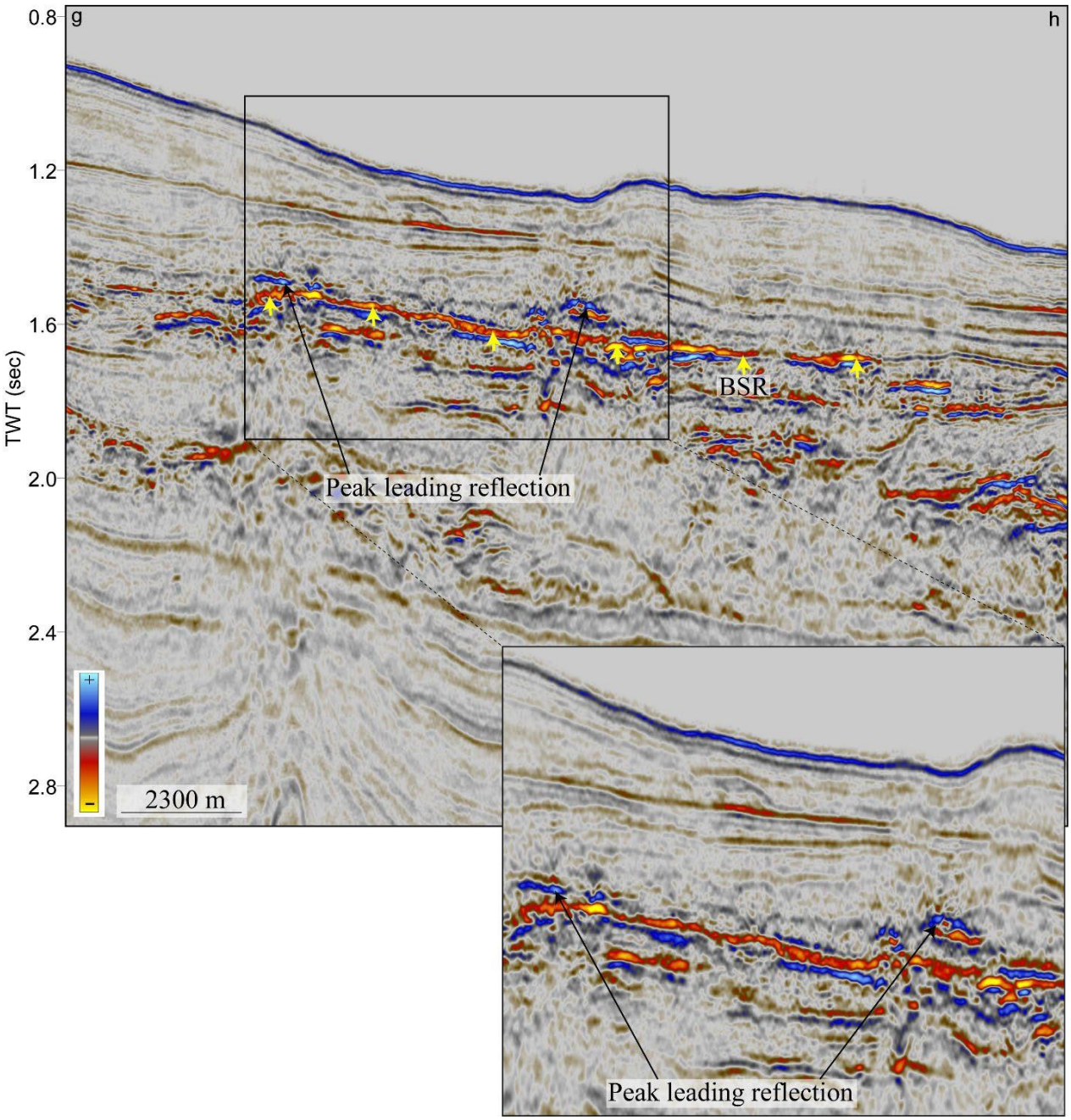

Figure 10: A seismic section showing a continuous BSR across the Eastern BSR system of Zone-1 in the Project Area 2.4. The profile location is shown in Figure 8.

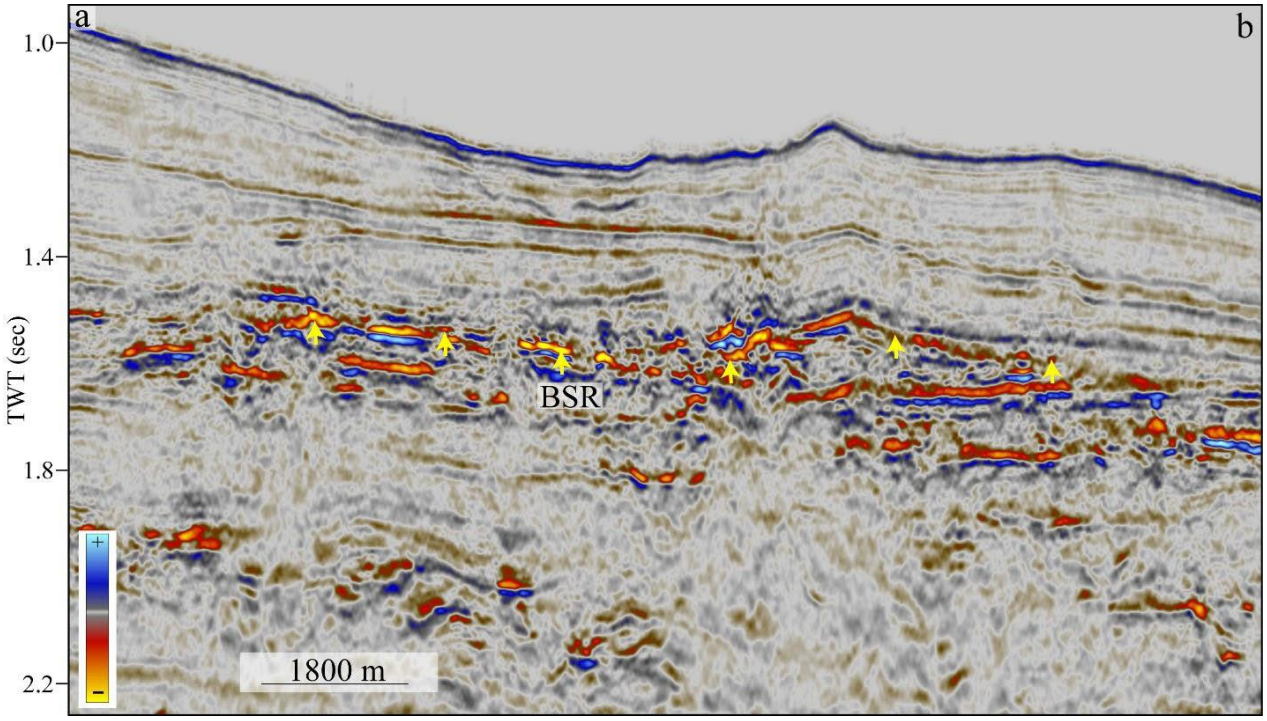

Figure 11: A seismic cross-section showing the BSR across the eastern BSR system of Zone-1. The profile location is shown in Figure 8.

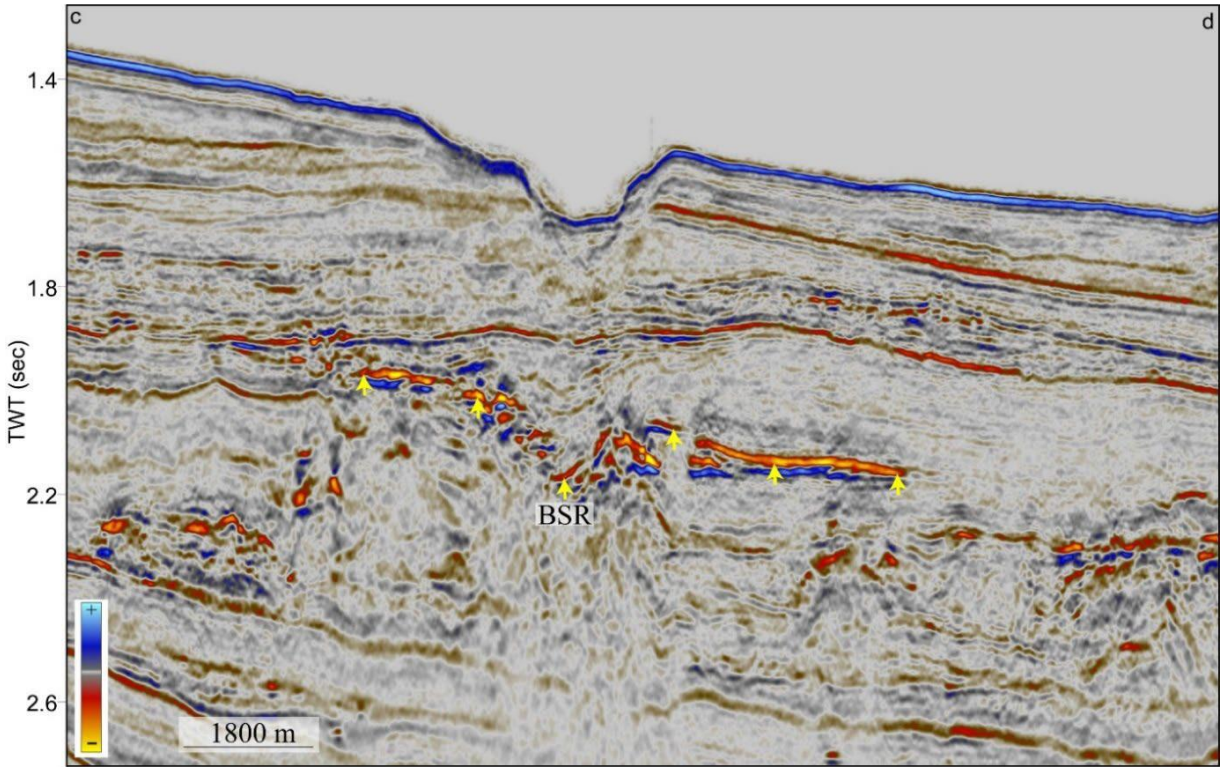

Figure 12: A seismic cross-section across southern BSR system of Zone-1 showing discontinuous BSR below the landslide escarpment. The profile location is shown in Figure 8.

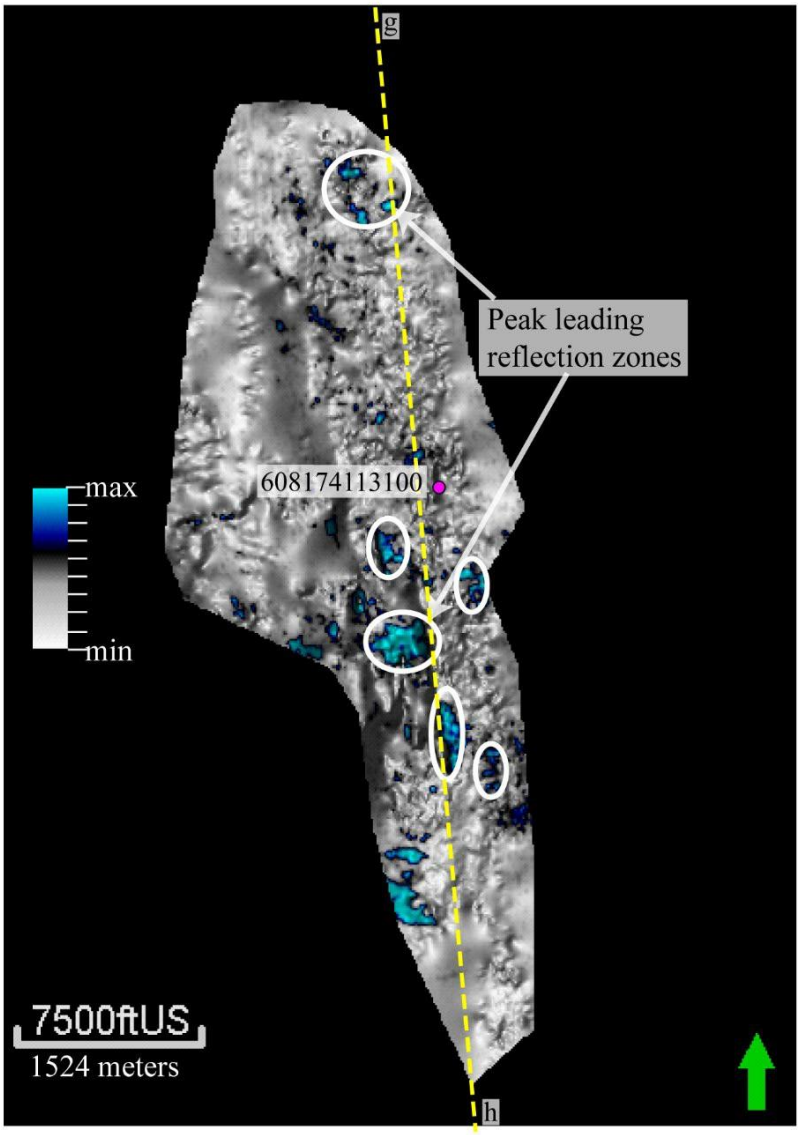

Figure 13: A map of average positive amplitude calculated within a 30 msec window above the BSRs in the eastern BSR system of Zone-1. Peak leading reflection zones are circled with white ellipses.

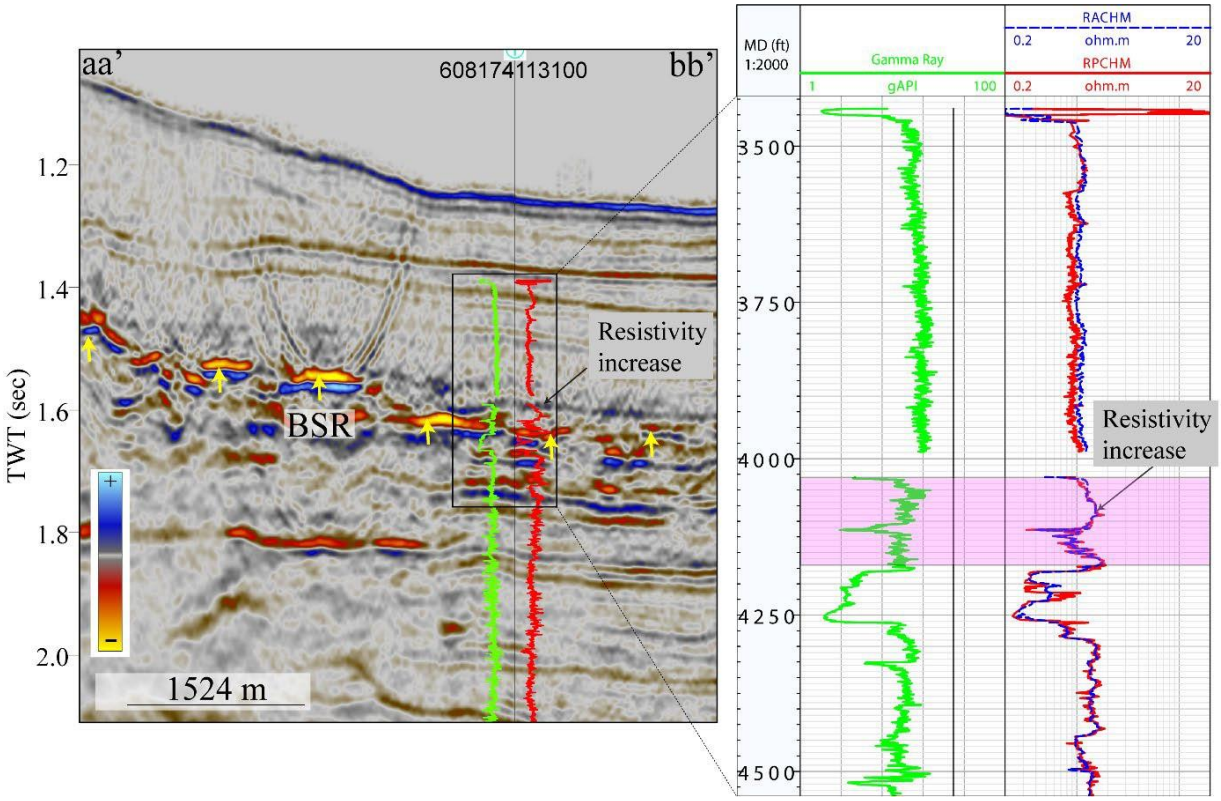

Figure 14: A seismic profile across the eastern BSR system of Zone-1 tied to the well API #608174113100. A slight increase in resistivity is observed above the BSR and just below the BSR. The profile location is shown *in Figure 8.*

Table 2: The seafloor depth, BSRs depth and geothermal gradient in the identified zones.

Zone	Seafloor Depth (m)	BSR depth below seafloor (m)	BSR depth from sea surface (m)	Seafloor TWT (msec)	BSR TWT (msec)	Geothermal Gradient (°C/km)
1	800 -1100	300 - 400	1100 -1500	1050 - 1450	1400 - 1900	25 - 30
2	1300 - 1500	200 - 450	1500 -1950	1700 - 2000	1870 - 2380	40 - 60
3	1500-1900	210 - 300	1710 - 2200	2000 - 2500	2250 - 2850	40 -70
4	1200 - 1750	250 - 450	1450 - 2200	1600 - 2300	1900 - 2850	35 - 55
5	1750 - 2100	225 - 350	1975 - 2450	2300 - 2800	2550 - 3200	50 - 70

4.2 Zone-2:

Zone-2 is located in the central part of Project Area 2.4 (Figure 2). We identify two BSR systems in this zone in water depths of 1300-1500 meters (Figure 15). The BSRs in the southwestern system show discontinuous characteristics, while the northeastern system shows clustered and continuous BSR characteristics (Figures 16, 17 and 18). Both systems are adjacent to or within two kilometers of a paleochannel (Figures 15 and 16).

The southwestern BSR system covers 16 km^2 and is associated with the salt diapir and Chandeleur Landslide (Figures 15 and 16). BOEM previously identified this BSR system, but its extent was larger than what we observe herein.

Figure 16 shows a seismic profile across the southwestern BSR system. A clear discontinuous BSR is observed along with a paleochannel feature on the eastern side. The paleochannel alongside this BSR system is mapped manually line-by-line. The BSR depth varies between 250-450 mbsf. The BSR is shallower in the southern part of this system due to the shallow salt. Prominent peak-leading reflections are observed above the BSRs in the southwestern BSR system (Figure 16). The average positive seismic amplitude map shows the extent of peak-leading reflection within this system (Figure 19).

The northeastern system is located above a salt diapir and spans a 15 km^2 area. The northeastern BSR system is mapped using two 3D seismic volumes, B-41-88-LA and B-49a-95-LA. The BSR in this zone is very shallow and lies between 200-250 meters below the seafloor. The paleochannel in the proximity of this zone is mapped manually, but the extension of this paleochannel is clearly seen in the RMS amplitude map of Zone-3 (Figure 20).

We estimate the geothermal gradient by assuming that the BSR is in a system with only methane gas. The geothermal gradient in the southwestern system in Zone-2 is ~40° C/km in the northern part and ~50° C/km on the southern side where BSR is shallower due to shoaling of salt. The geothermal gradient in the northeastern system of Zone-2 is significantly higher at ~ 60°C/km. This high geothermal gradient is attributed to the shallowing of the salt in this region (Figure 17, 18).

There are no wells drilled in Zone-2 close to the BSR systems.

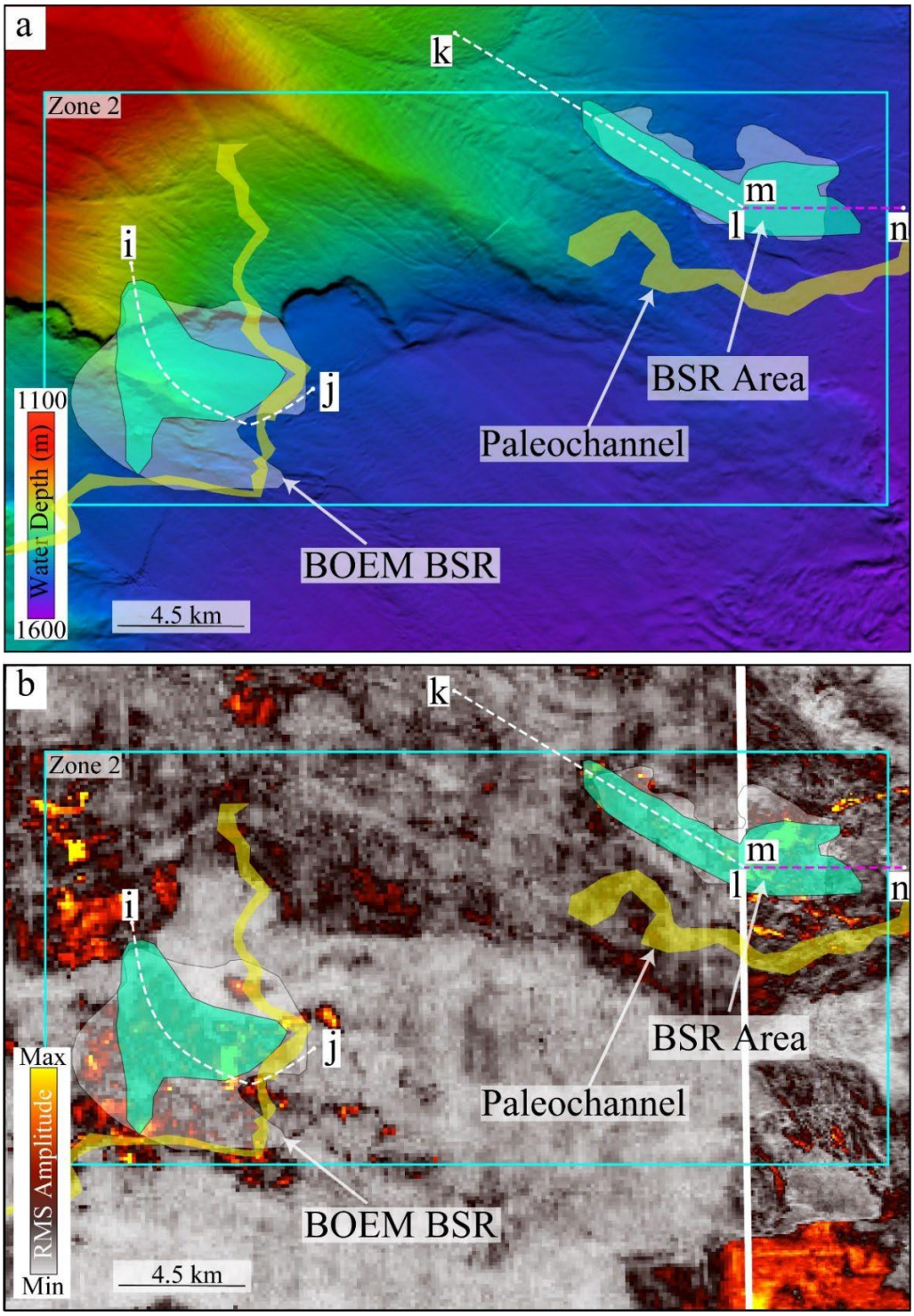

Figure 15: a) A bathymetry map showing the BSR extent within Zone-2 of Project Area 2.4. Yellow coloring shows the interpreted paleochannels. b) A RMS amplitude map of the sub-seafloor interval between 350-450 msec. White and purple dashed lines show the locations of arbitrary seismic lines shown in the following figures.

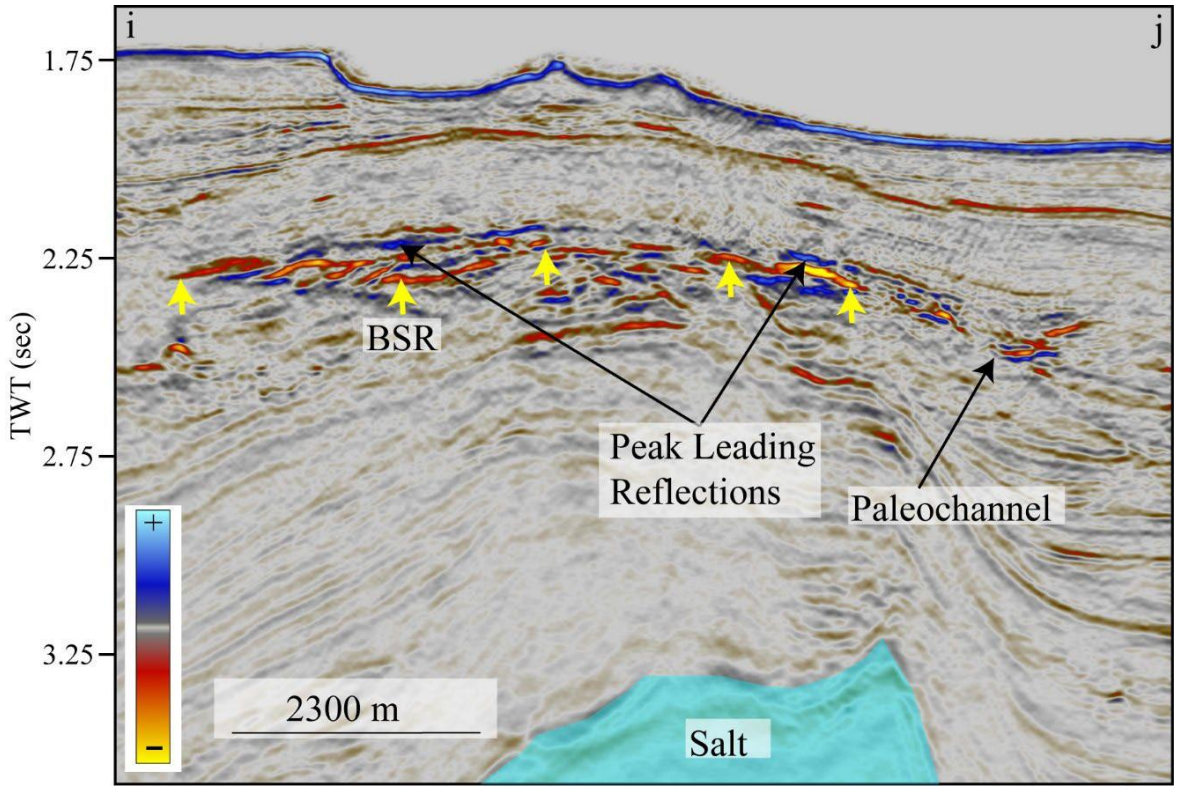

Figure 16: A seismic profile showing a discontinuous BSR below the landslide across southwestern BSR system of Zone-2. A few peak-leading reflections are observed above the interpreted BSR. The salt diapir and paleochannel features are also shown in the profile. The profile location is shown in Figure 15.

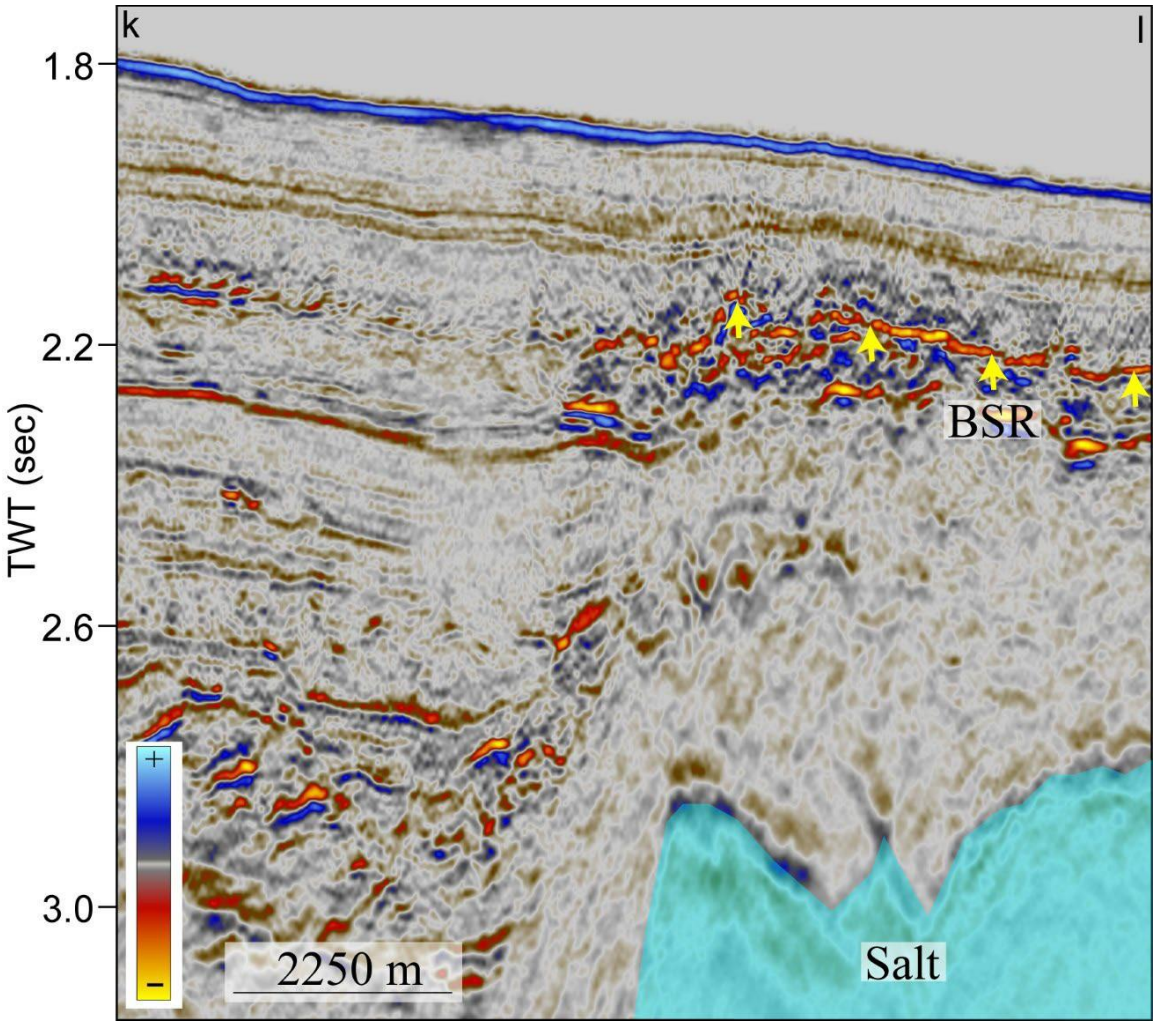

Figure 17: A seismic profile across the northeastern BSR system of Zone-2 showing the BSR above the salt body. The profile location is shown in Figure 15.

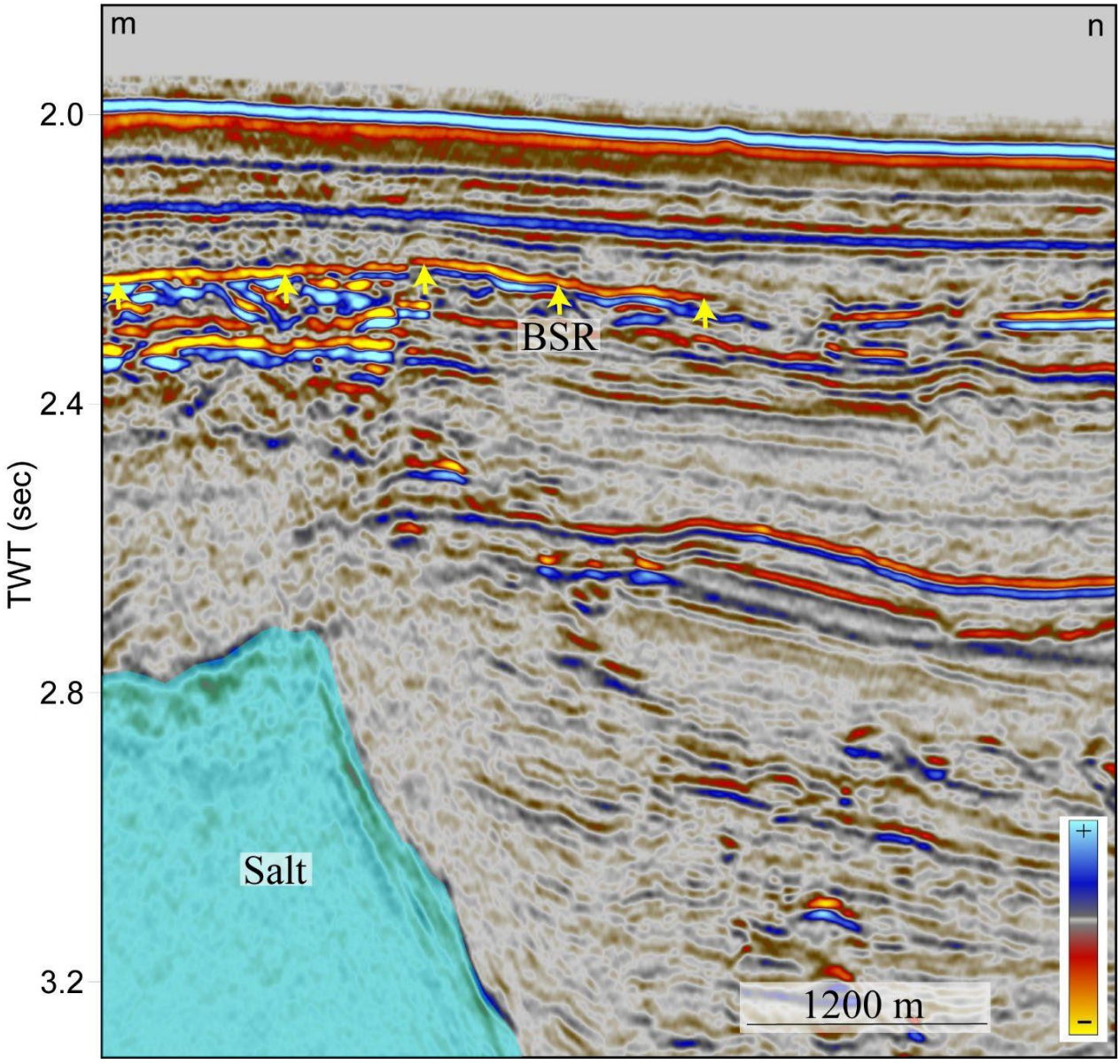

Figure 18: A seismic profile across the northeastern BSR system of Zone-2 showing clustered BSR above the salt body. The profile location in Figure 15.

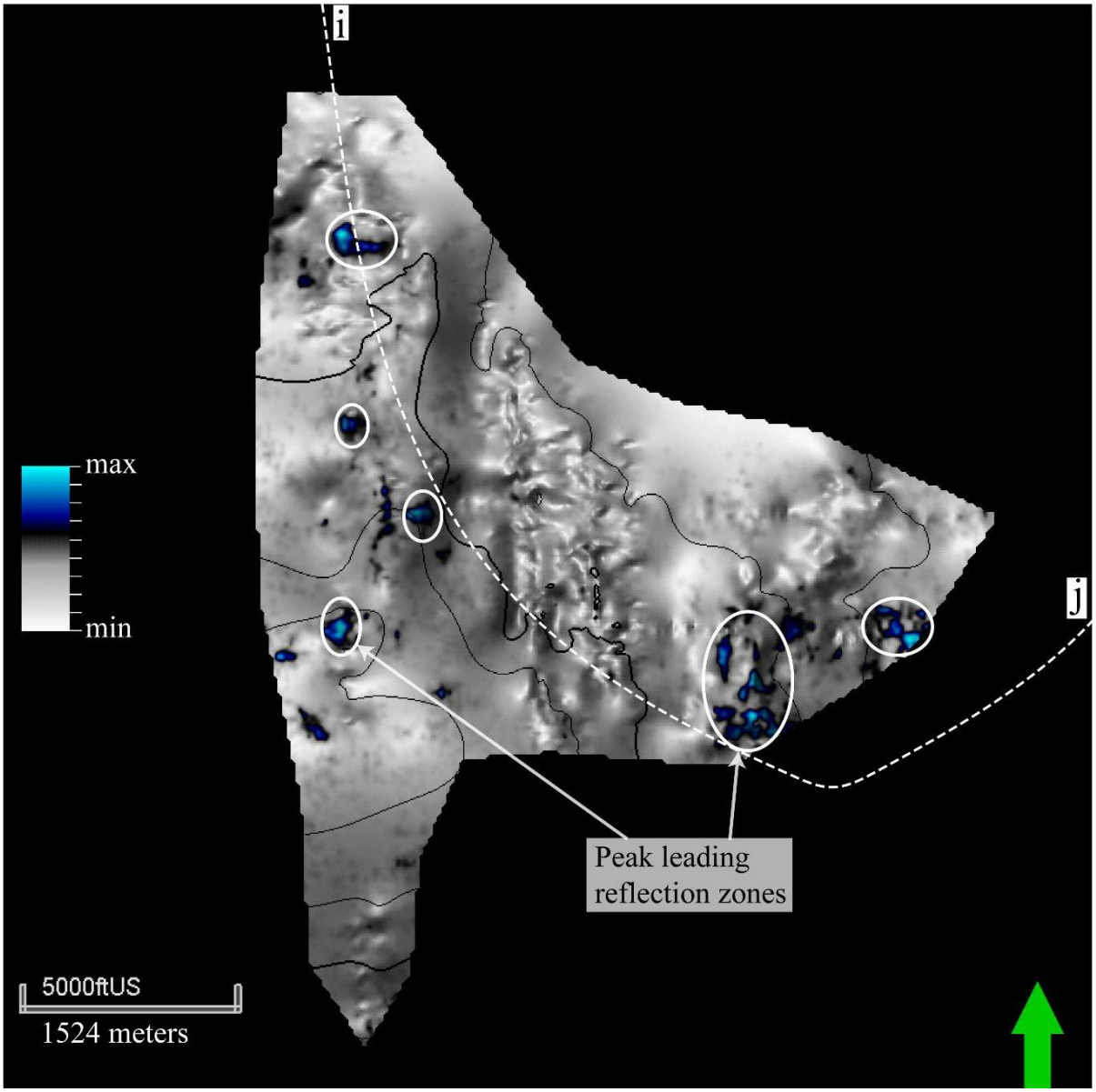

Figure 19: A map of average positive amplitude calculated within a 30 msec window above the BSRs in the southwestern BSR system of Zone-2. Peak leading reflection zones are circled with ellipses.

4.3 Zone-3:

Zone-3 is located in the eastern part of Project Area 2.4 (Figure 2). Two large BSR systems are identified in this zone, southwestern and northeastern, and both systems are near a paleochannel (Figure 20). The systems span 43 km^2 and 38 km^2, respectively. Both systems are located over salt diapirs (Figures 20-26). The BSRs are clustered in nature above the salt diapirs and become continuous and discontinuous BSRs as they extend away from the salt (Figure 21, 24). The northeastern system is newly identified and was not previously mapped. Water depth in this zone varies between 1500-1900 m (Figure 20). The southwestern system is highly faulted, probably due to the shallowing of the salt (Figure 21). For the same reason, the BSRs shoal towards the seafloor and does not follow the seafloor topography (Figure 21). To map the fault pattern, Horizon H1 (Figure 21) above the BSR is mapped, which shows the east-west trending faults in the area (Figure 23).

BSRs in this zone are present between 250-350 msec TWT (~210 – 300 m) below the seafloor. BSRs most likely become shallower above the diapir due to a higher geothermal gradient. The minimum geothermal gradient in this zone is estimated to be ~40° C/km away from the salt diapir and reaches a maximum of ~70° C/km above the summit of the diapir (assuming purely methane gas composition).

One well, well API #608174103700, was drilled at the edge of this BSR in the southwestern system. However, no high resistivity is observed within the zone of interest. We did not tie the well logs to seismic data for this well because the logs are only available in pdf format.

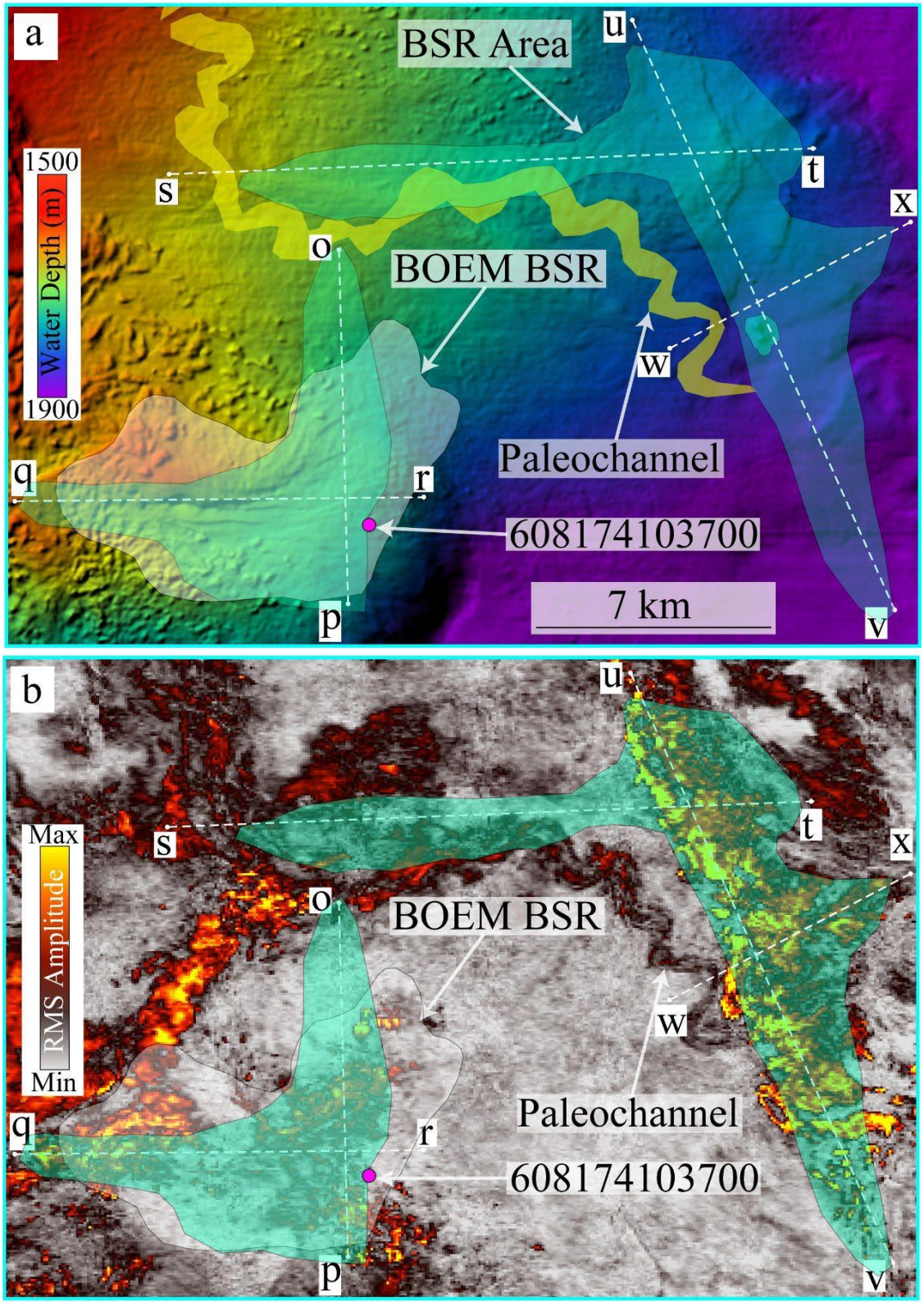

Figure 20: a) A bathymetry map showing the BSR extent within Zone-3 of Project Area 2.4. Yellow coloring shows the location of the paleochannel. b) A RMS amplitude map of the sub seafloor interval between 350-450 msec. White dashed lines show the locations of arbitrary seismic lines shown in the following figures.

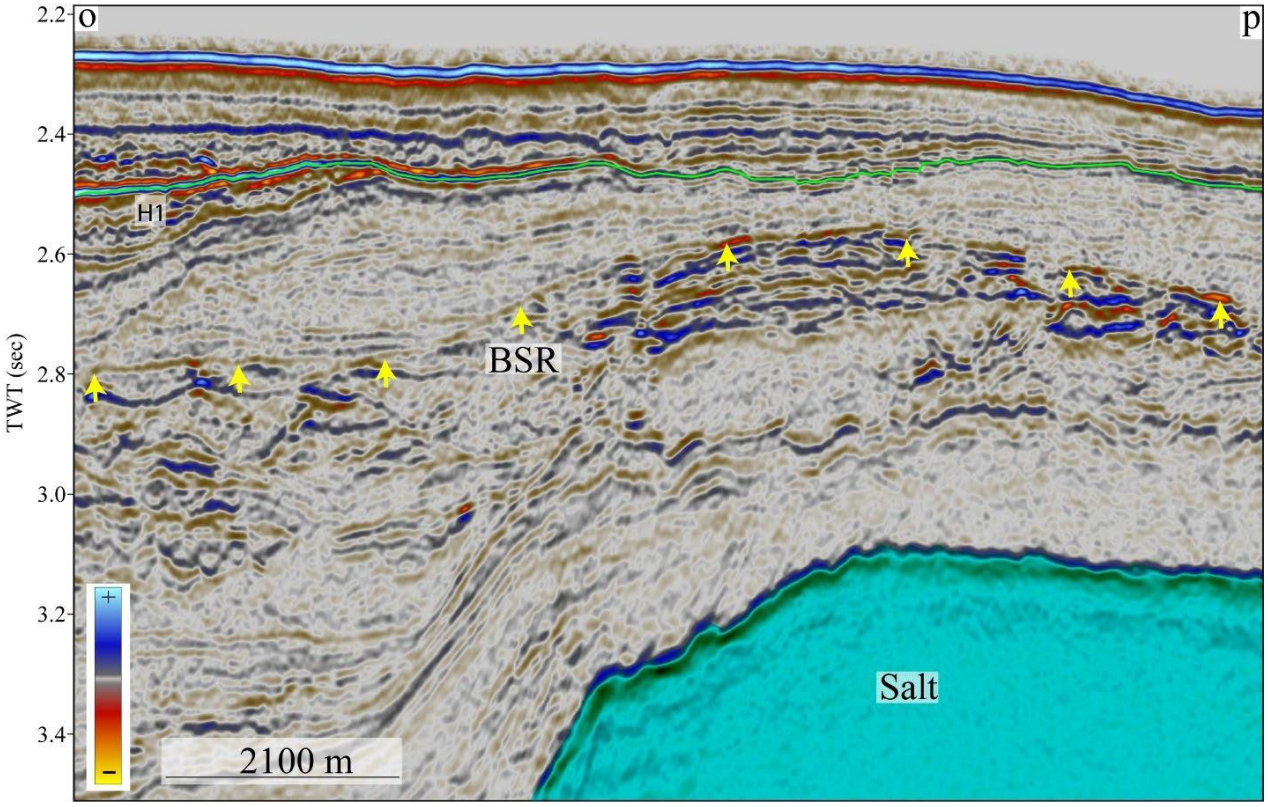

Figure 21: The seismic profile shows the north-south cross-section across southeastern BSR system of Zone-3. A clustered BSR is observed above the salt diapir and a weak continuous BSR away from the salt diapir. Horizon H1 is mapped just above the BSR. The profile location is shown in Figure 20.

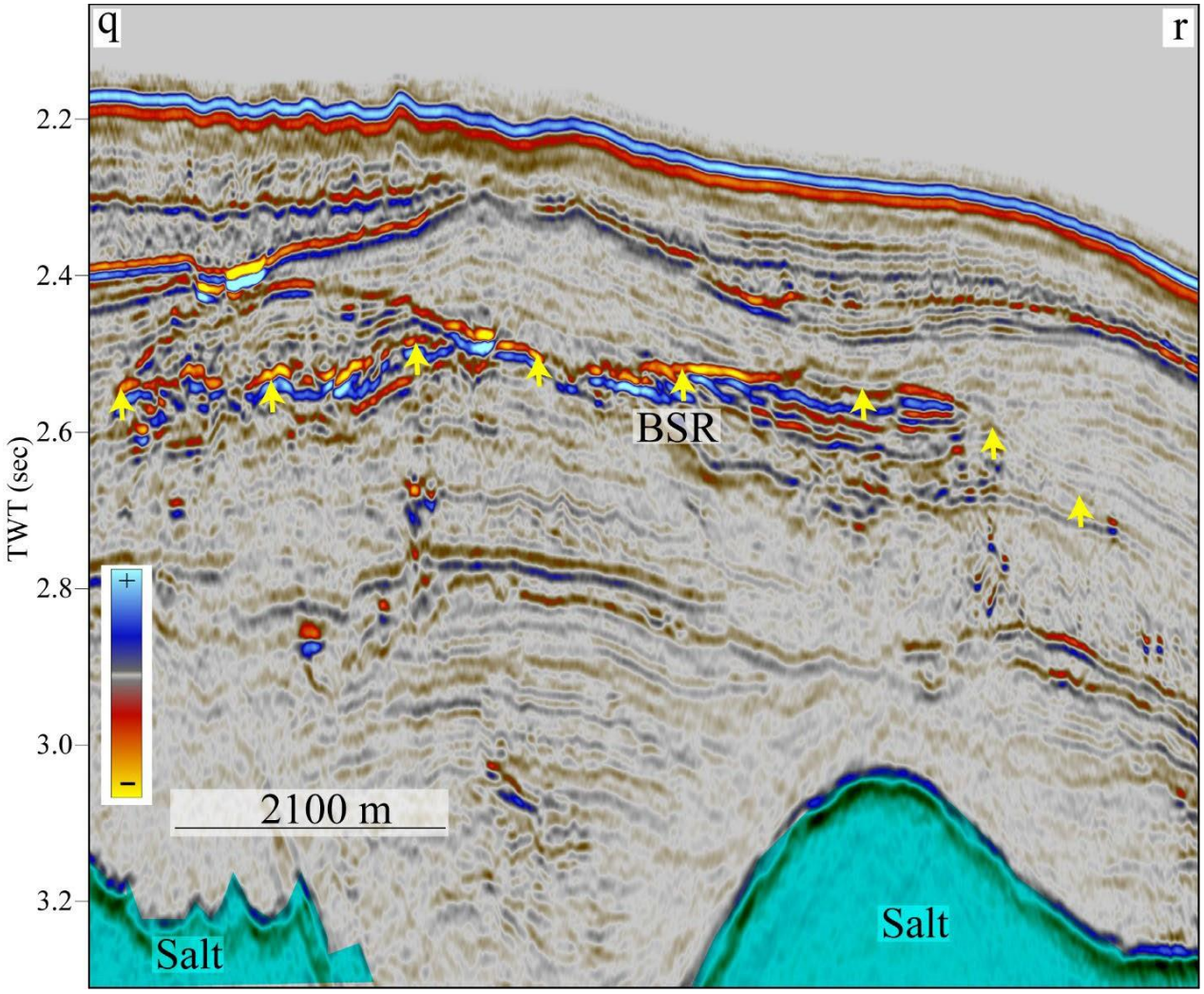

Figure 22: A seismic profile showing the east-west cross-section across the southwestern BSR system of Zone-3. The profile location is shown in Figure 20.

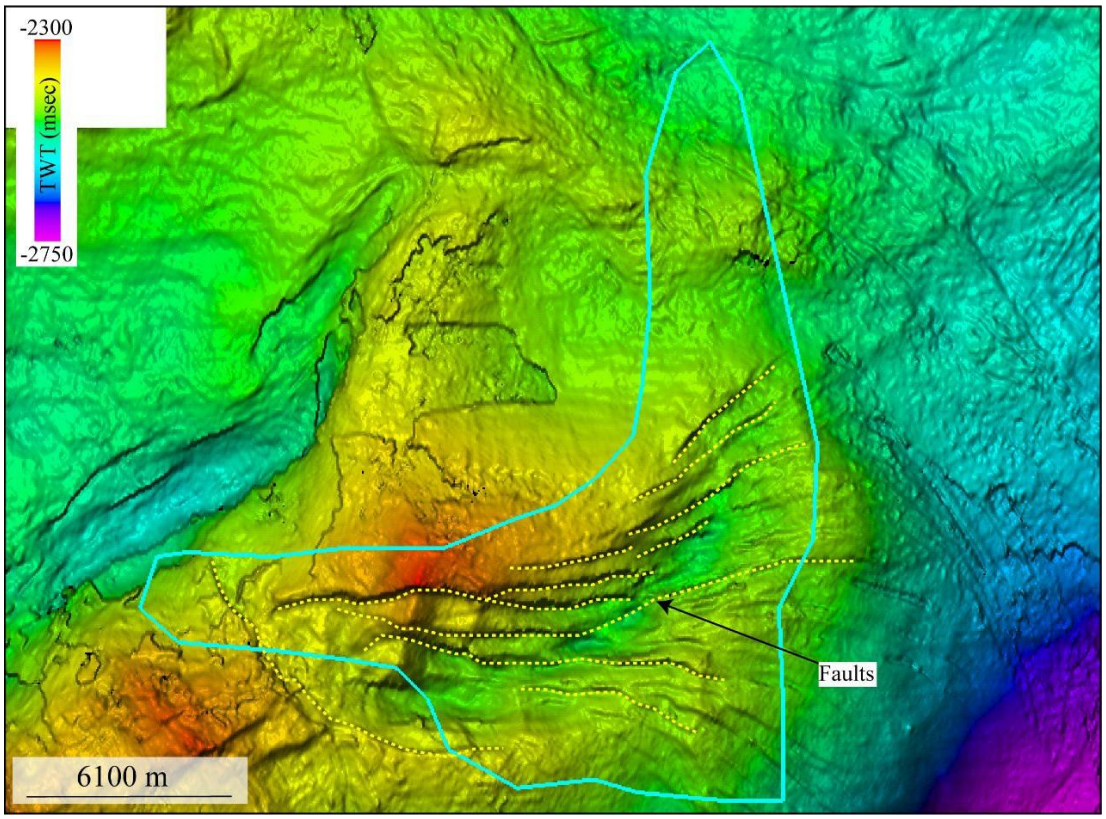

Figure 23: Time-structure map of Horizon H1 (Figure 21) above the BSR in the south-western BSR system of Zone-3. Yellow dashed lines show the faults interpreted within the BSR system.

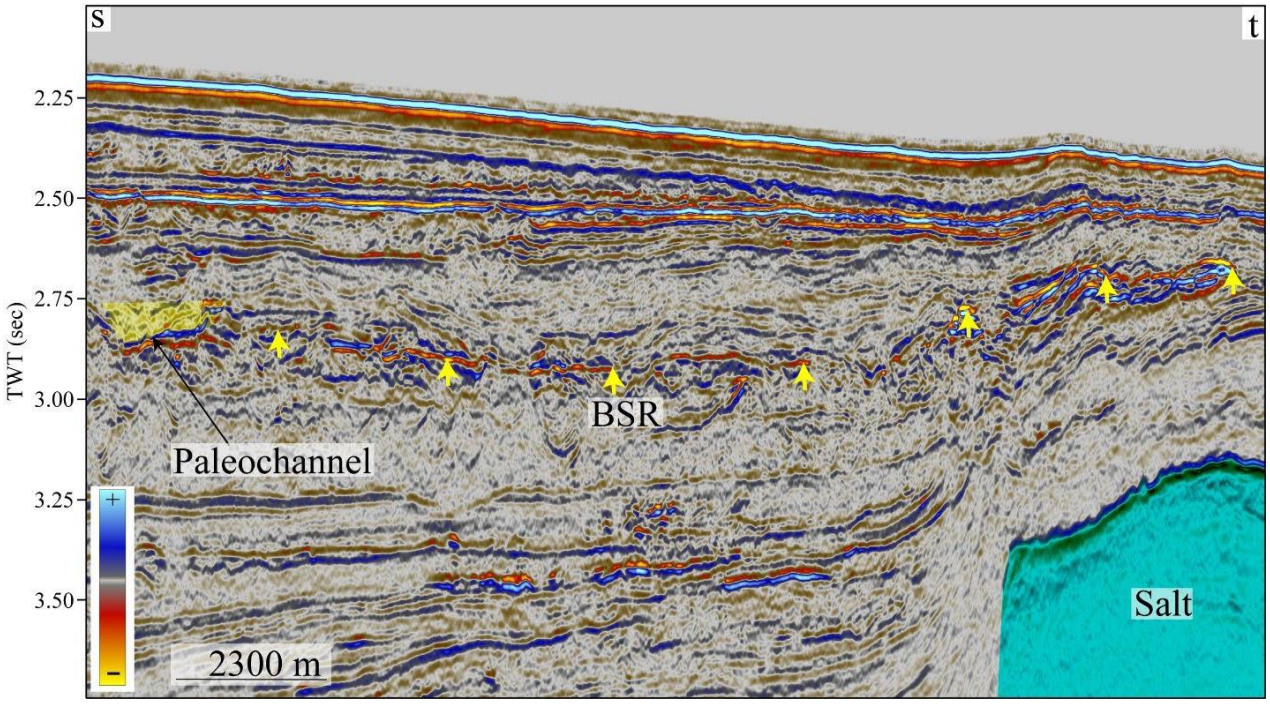

Figure 24: A seismic profile showing east-west cross-section across the north-eastern BSR system of Zone-3. The profile location is shown in Figure 20.

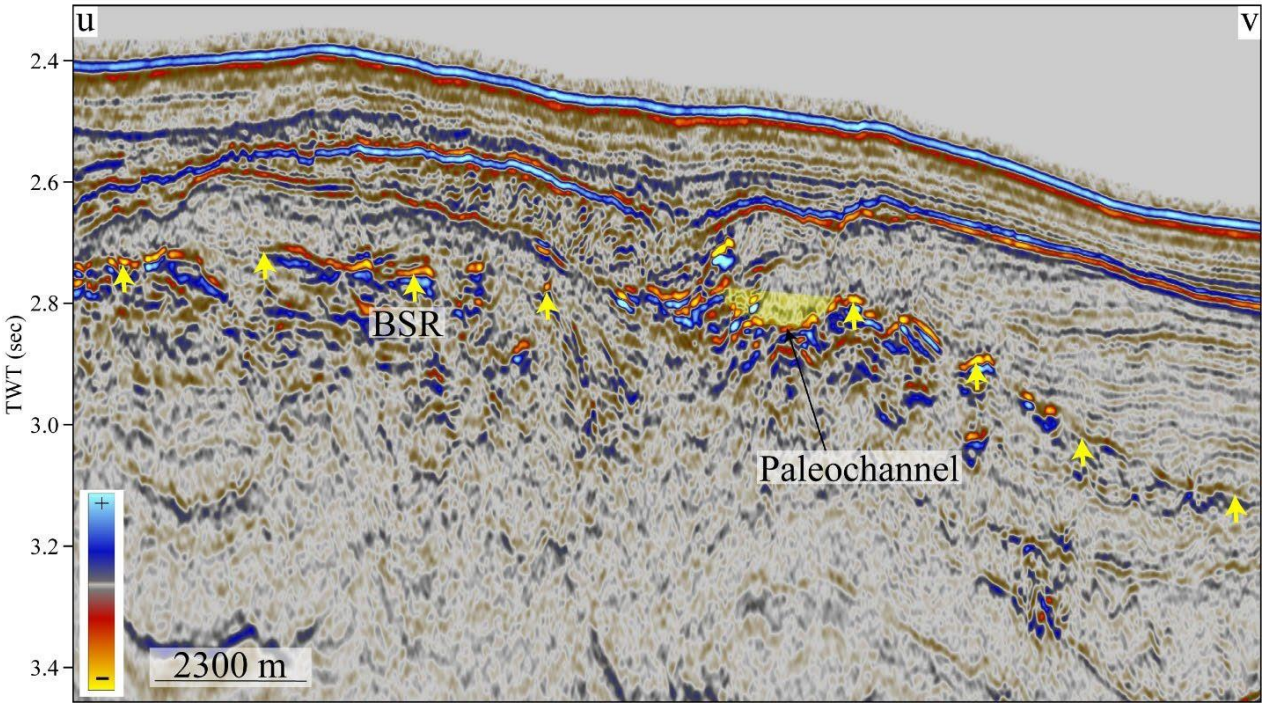

Figure 25: A seismic profile showing north-south cross-section of north-eastern BSR system of Zone-3. The profile location is shown in Figure 20.

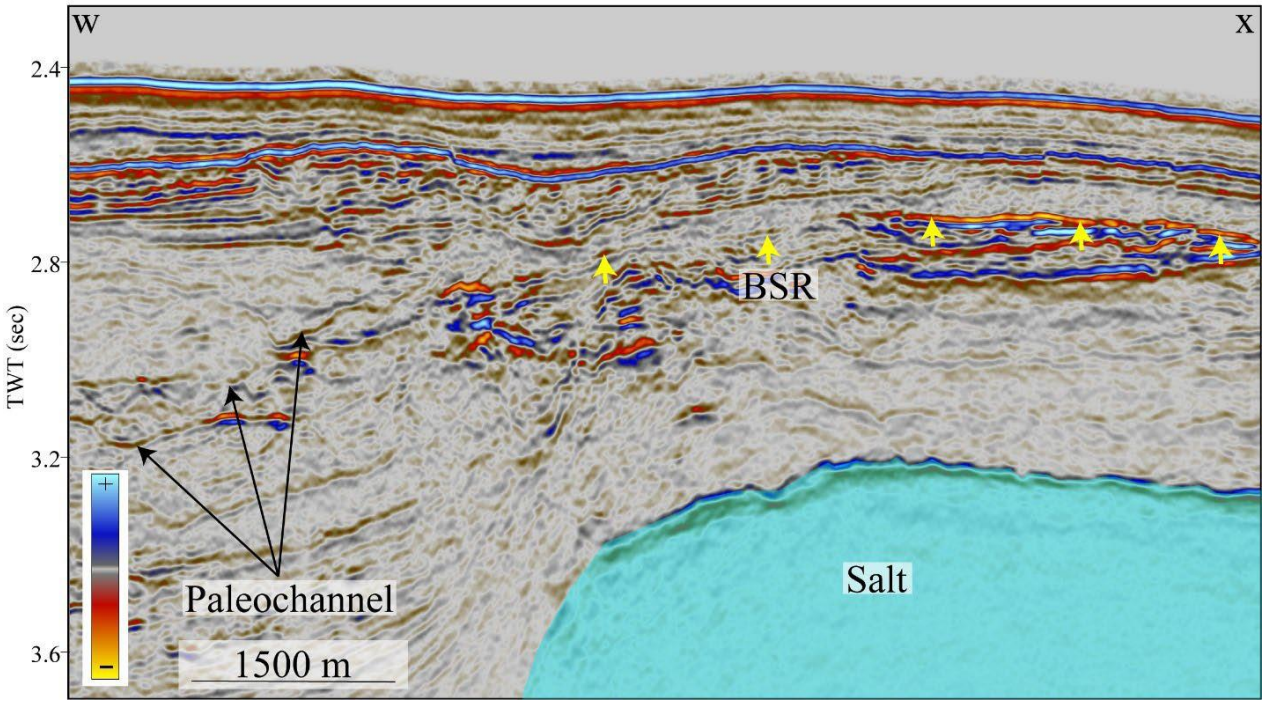

Figure 26: A seismic profile showing a clustered BSR near the paleochannel in Zone-3. The profile location is shown in Figure 20.

4.4 Zone-4:

Zone-4 is located in the southwestern part of the Project Area 2.4 (Figure 2). We identify five BSR systems in this zone that are present in water depths of 1200 – 1750 m (Figure 27). This zone is characterized by major landslides, salt diapirs and salt ridges. The BSR systems on the east and west side of Zone-4 are newly reported and were not previously identified. BOEM identified the BSR system in the north, but its extent was limited to a smaller area; the new system is significantly expanded to the east (Figure 27). The BSR systems in the north, west and east span an area of 45 km^2, 21 km^2 and 9 km^2, respectively. The two BSR systems in the south are both ~7 km^2. All the BSR systems are present above salt structures (Figure 28-33). Salt movement has caused extensive faulting in Zone-4.

The eastern BSR system shows a prominent clustered BSR over the salt mound (Figure 31). We map Horizon H2 above the BSR system to understand the structural control over the eastern BSR system (Figure 32). Salt rise has uplifted the sediments locally and opened up several local fault systems, as observed in Figure 32. These local fault systems may be responsible for the migration of free gas to the hydrate stability zone and result in the formation of the clustered BSRs. Clustered BSRs also observed in the southernmost BSR system (Figure 29).

Two wells, API #608174133700 and API #608174130100, were drilled near the northern and eastern BSR systems, respectively (Figure 27). Figure 34 shows Well #608174133700 tied to the seismic cross-section. A spike in the resistivity is observed just above the BSR, likely indicating the presence of gas hydrates or free gas. Well #608174130100 is drilled at the edge of the interpreted eastern BSR (Figure 35) and does not show any increase in the resistivity within the zone of interest.

Three out of five BSRs are close to paleochannels (Figure 27). Paleochannels in Zone-4 are mapped manually based on line-by-line interpretation (Figure 29, 33). A paleochannel close to a BSR suggests that there may be a higher chance of a coarse-grained reservoir associated with the BSR; however, due to the absence of the well log data in the vicinity of the paleochannels, it is not possible to confirm the presence of sand.

The BSR depth varies between ~250-450 meters below the seafloor in Zone-4. The geothermal gradient Zone-4 is estimated to be between 35° C/km to ~55° C/km (Table 2). The geothermal gradient is high where salt is shallow.

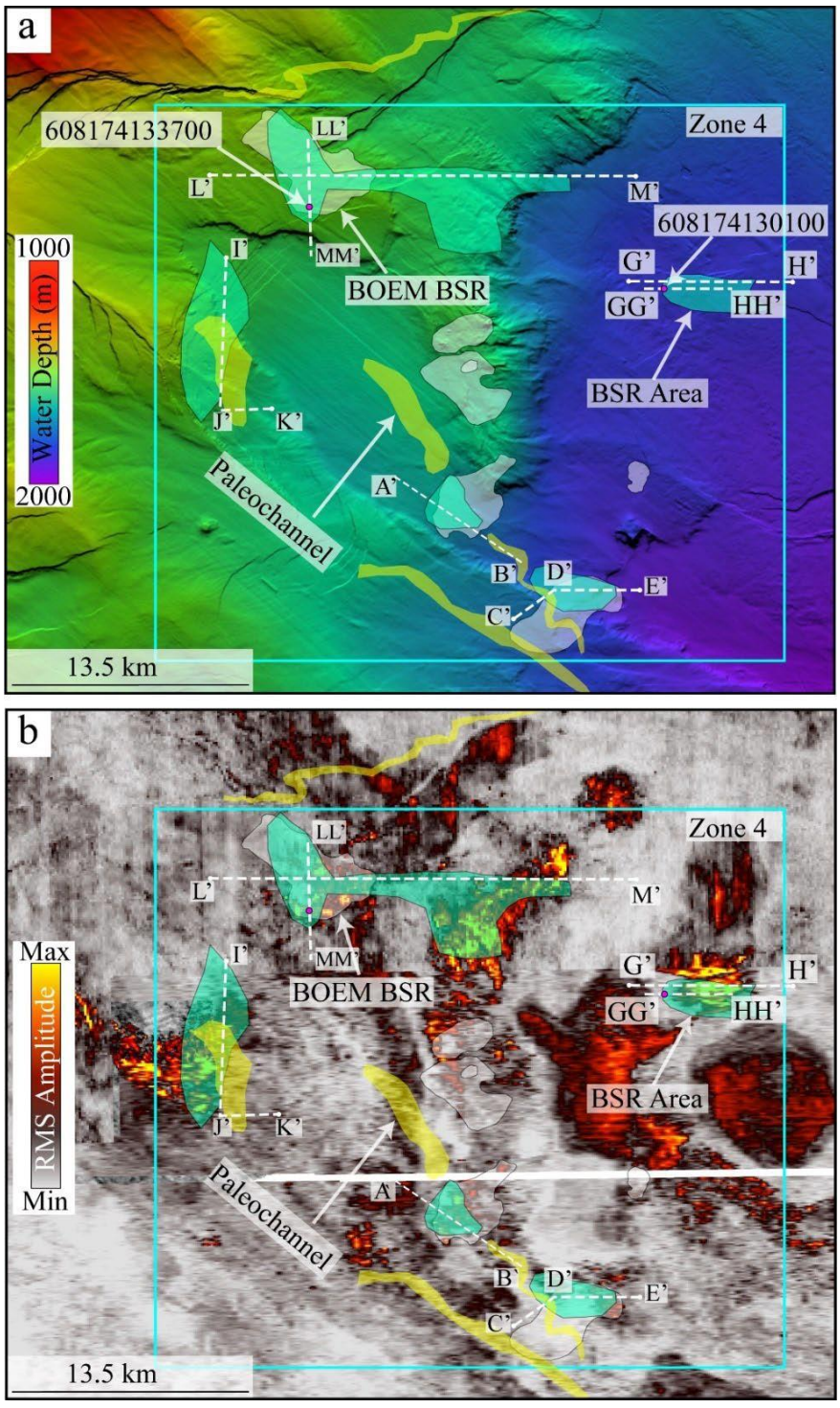

Figure 27: a) A bathymetry map showing the BSR extent within Zone-4 of Project Area 2.4. Yellow coloring shows the locations of paleochannels. b) An RMS amplitude map of the sub-seafloor interval between 350-450 msec. White dashed lines show the locations of arbitrary seismic lines shown in the following figures.

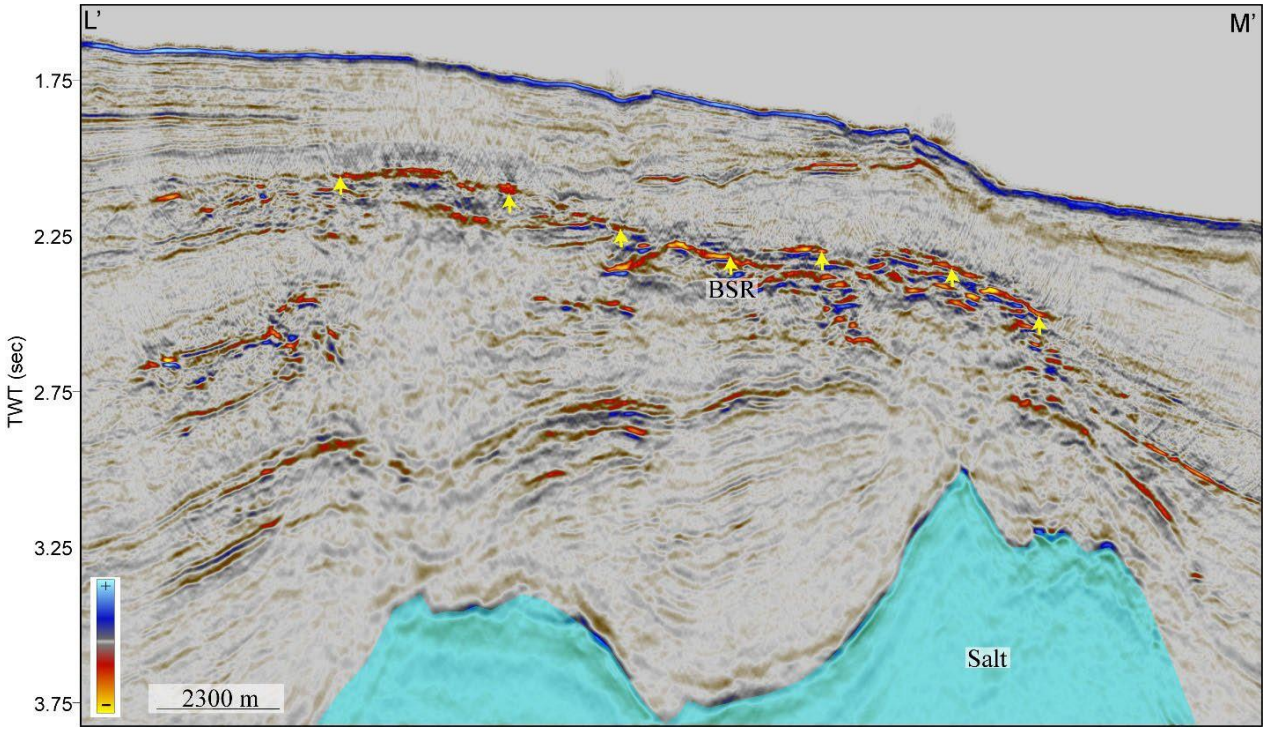

Figure 28: A seismic profile showing the discontinuous BSR across the northern BSR system of Zone-4. The profile location is shown in Figure 27.

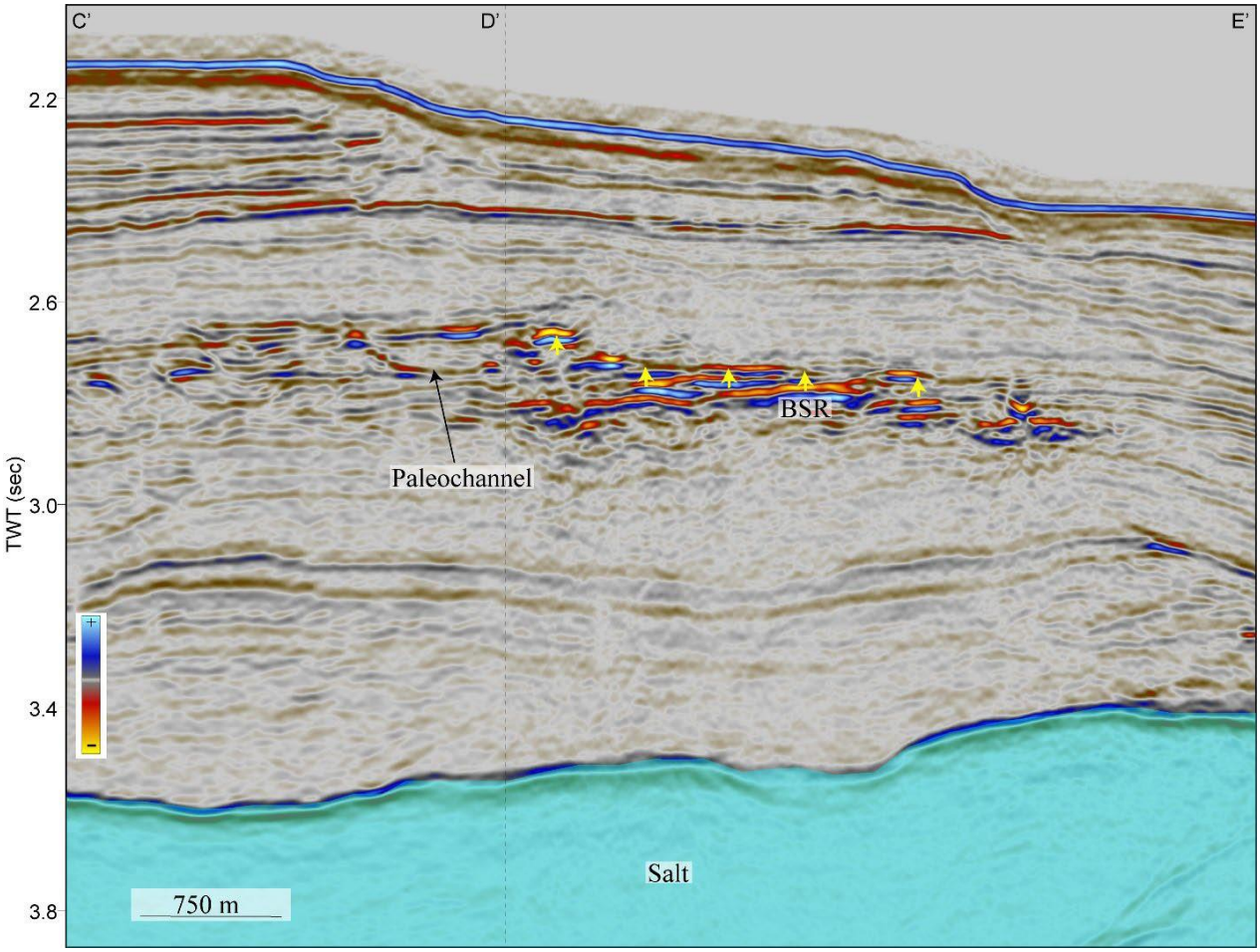

Figure 29: A seismic profile across the southernmost clustered BSR system of Zone-4. The profile location is shown in Figure 27.

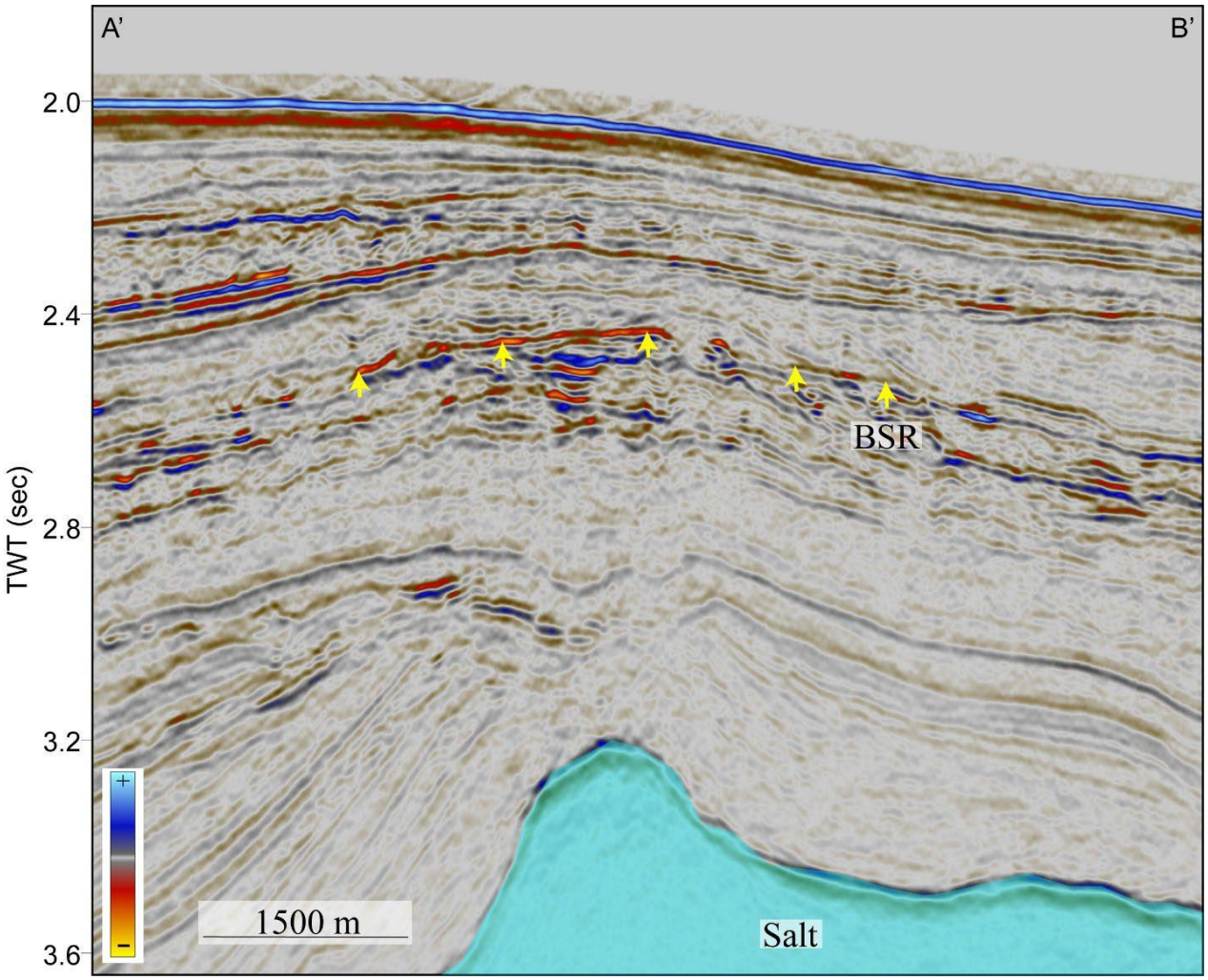

Figure 30: A seismic profile showing continuous BSR across the BSR system at the center of Zone-4. The profile location is shown in Figure 27.

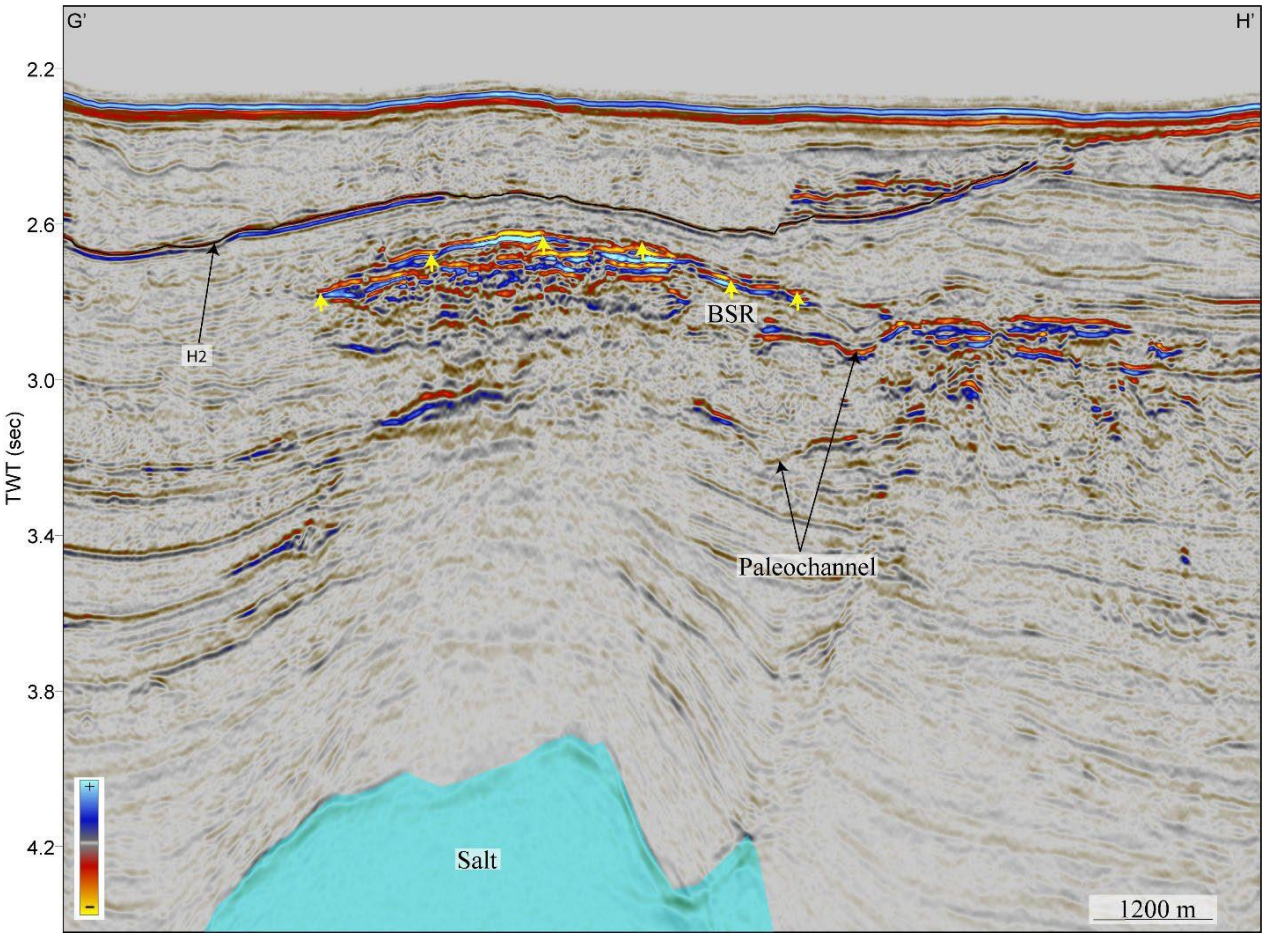

Figure 31: A seismic profile across the eastern BSR system in Zone-4 showing the clustered BSR above the salt diapir. Paleochannel signatures are observed in the seismic section. Horizon H2 used for time-structure map is interpreted above this BSR. The profile location is shown in Figure 27.

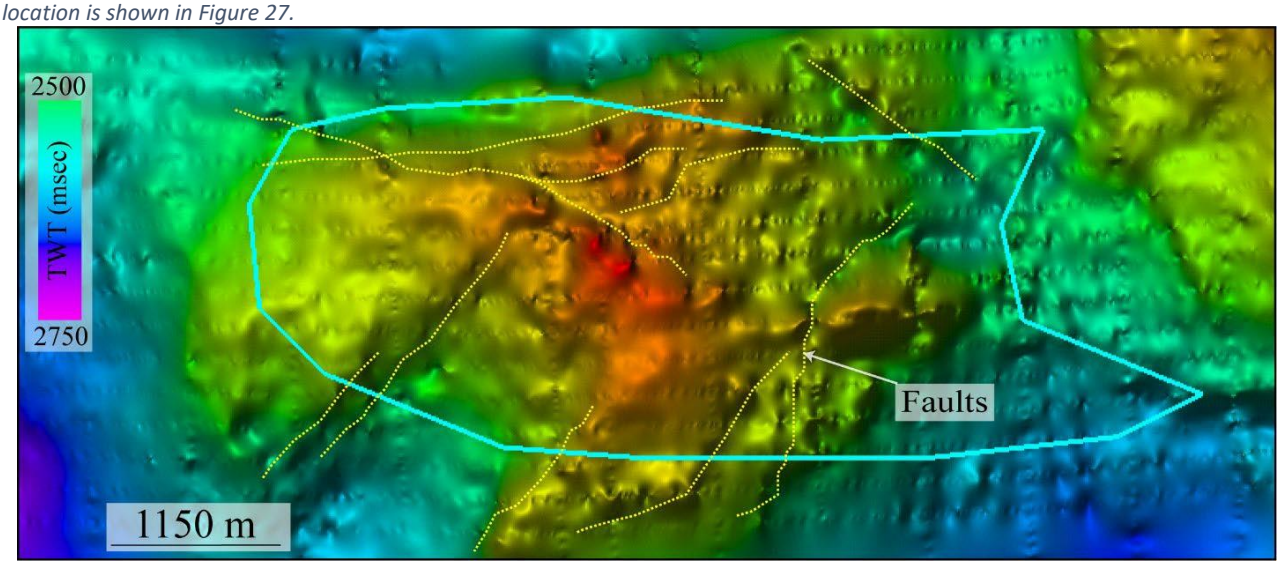

Figure 32: A time-structure map of Horizon H2 (Figure 31) above the BSR in the eastern BSR system of Zone-4. Yellow dashed lines show the interpreted fault within the BSR system

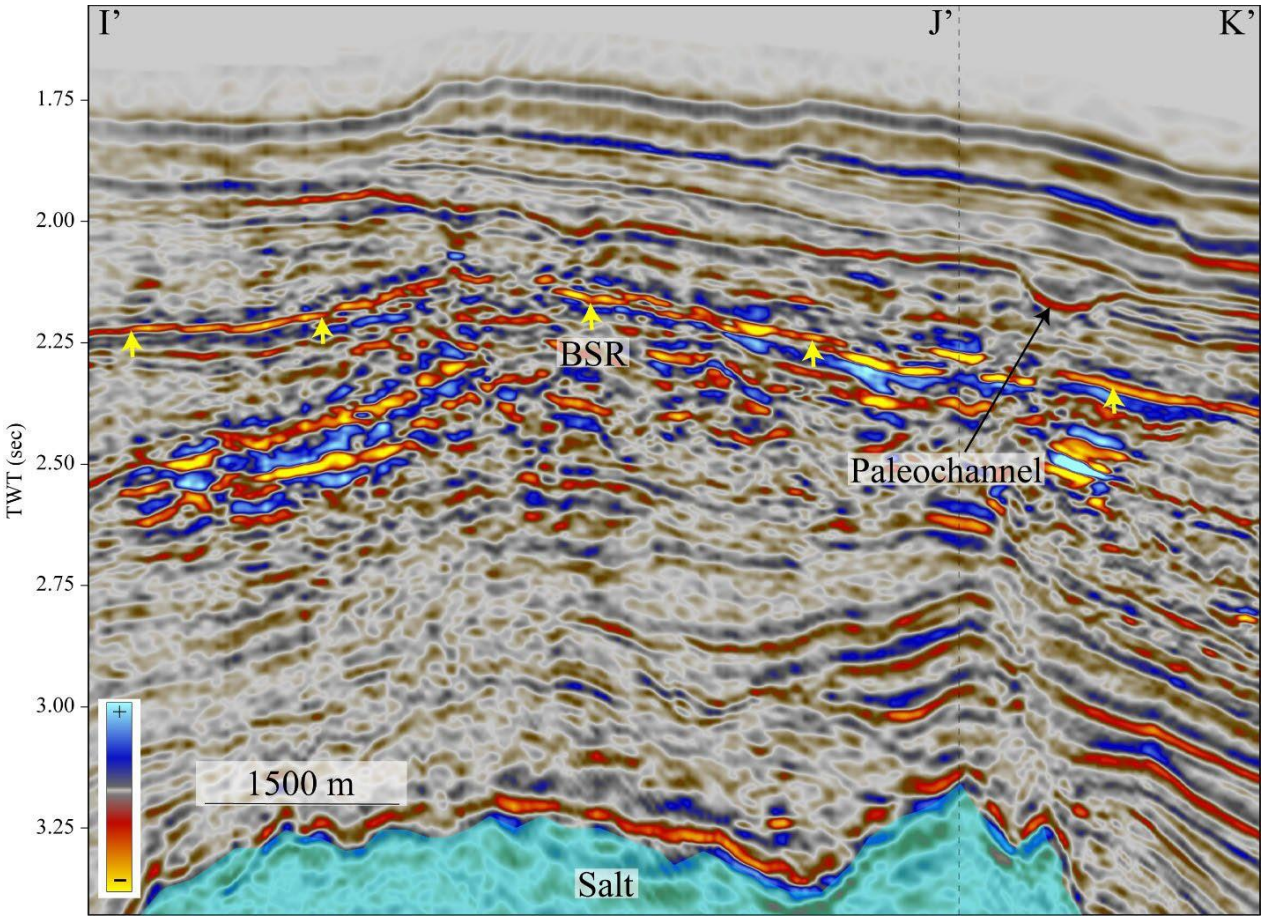

Figure 33: A seismic profile across the western BSR system of Zone-4 showing a continuous/clustered BSRs along the profile. The profile location is shown in Figure 27.

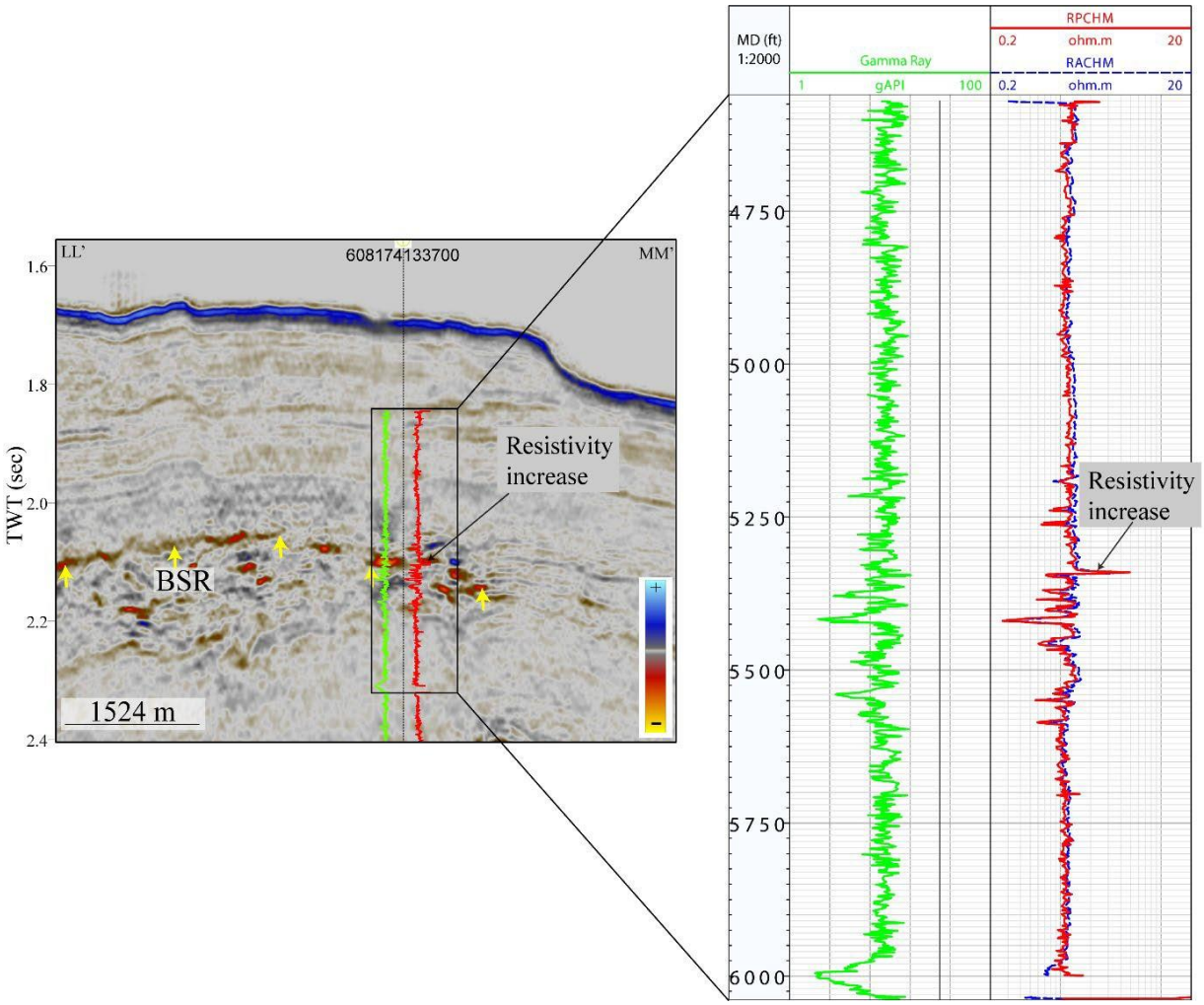

Figure 34: Well #608174133700 tied to the seismic profile. A high resistivity spike is observed just at the BSR depth and probably indicates the presence of the gas hydrates or free gas. The profile location is shown in Figure 27.

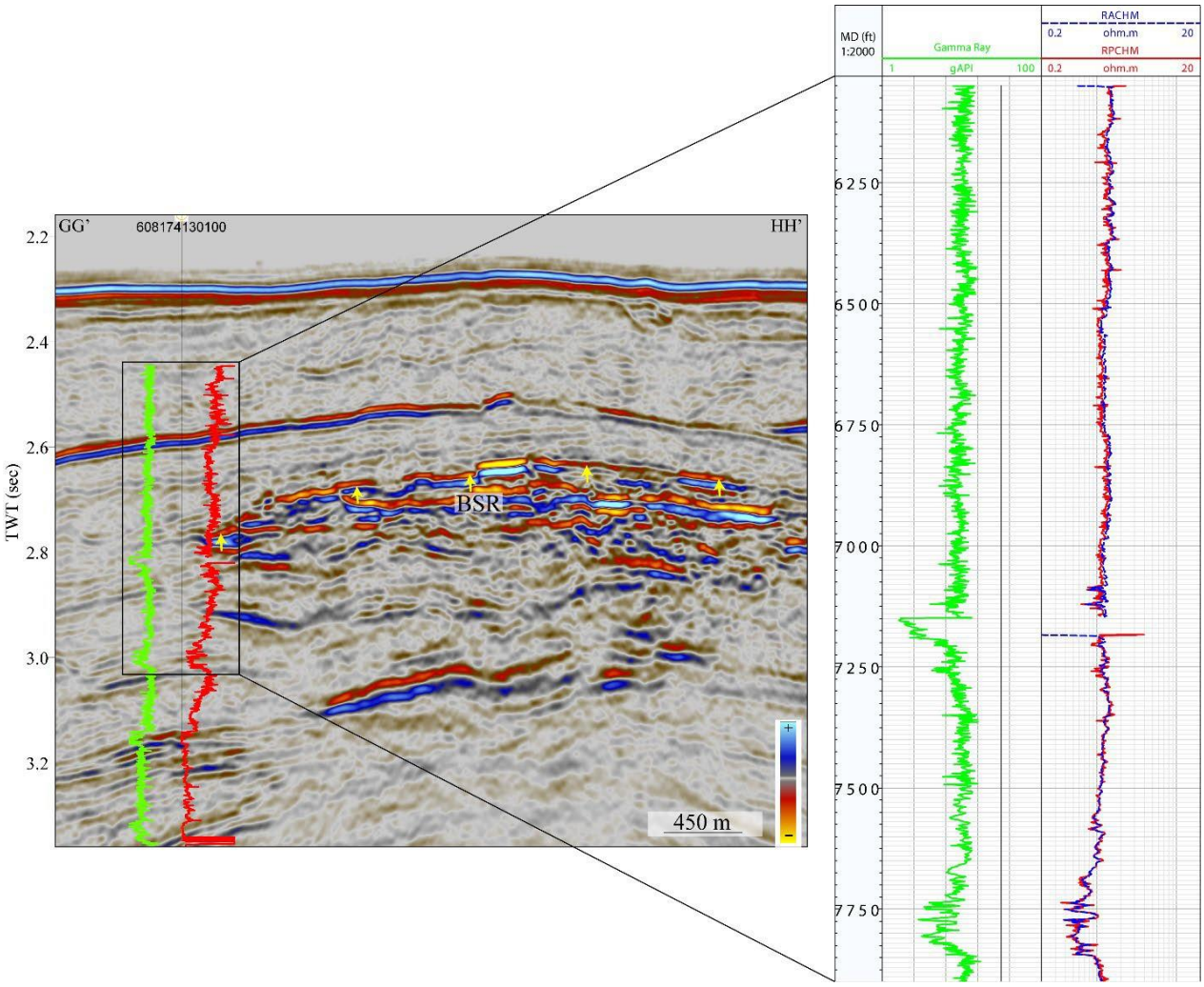

Figure 35: Well API #608174130100 tied with the seismic cross-section across the eastern BSR system of Zone-4. The resistivity log (red solid curve) show no increase in the resistivity. The well is just outside the BSR system. The profile location is shown in Figure 27.

4.5 Zone-5:

Zone-5 is located in the southeast part of Project Area 2.4 (Figure 2). Water depth in this zone varies between 1750 – 2100 meters (Figure 36). We identify two BSR systems in Zone-5, one in the west and one in the east, covering 40 km^2 and 17 km^2, respectively (Figure 36). Both systems are easily identified in the RMS amplitude map (Figure 36b). These clustered BSRs are located over the salt diapir (Figures 37 and 38).

The BSRs in Zone-5 occur within 2.7 to 3.2 s TWT below sea level. The BSRs are shallower above the salt and deepen away from the salt diapirs. The seismic profile over the eastern BSR system shows a clear correlation between the salt and the BSR depth (Figure 38). The clustered BSR systems of Zone-5 are within four-way closure structures formed due to the uplifting of salt.

BSRs are commonly observed between ~225-350 meters below the seafloor. The geothermal gradient in this zone is estimated to be between ~40° C/km to ~70° C/km. The geothermal gradient is the highest at the center of the eastern BSR system. Fluid flow along the fault system and shallow salt is likely responsible for such a high geothermal gradient.

No well log data is available near the BSR systems in Zone-5.

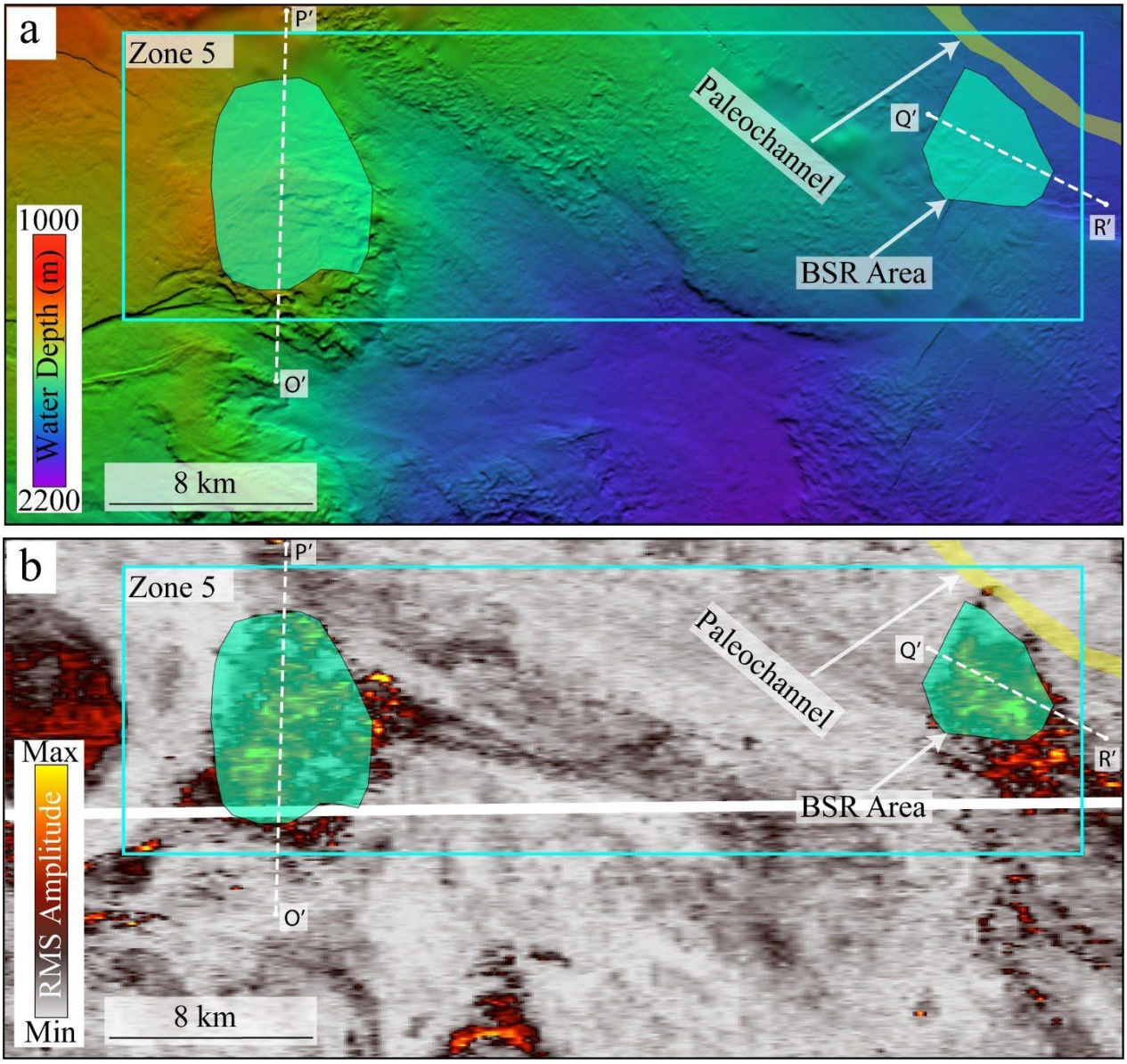

Figure 36: a) A bathymetry map showing the BSR extent within Zone-5 of Project Area 2.4. Yellow coloring shows the location of the paleochannel. b) A RMS amplitude map of the sub-seafloor interval between 350-450 msec. White dashed lines show the locations of arbitrary seismic lines shown in the following figures.

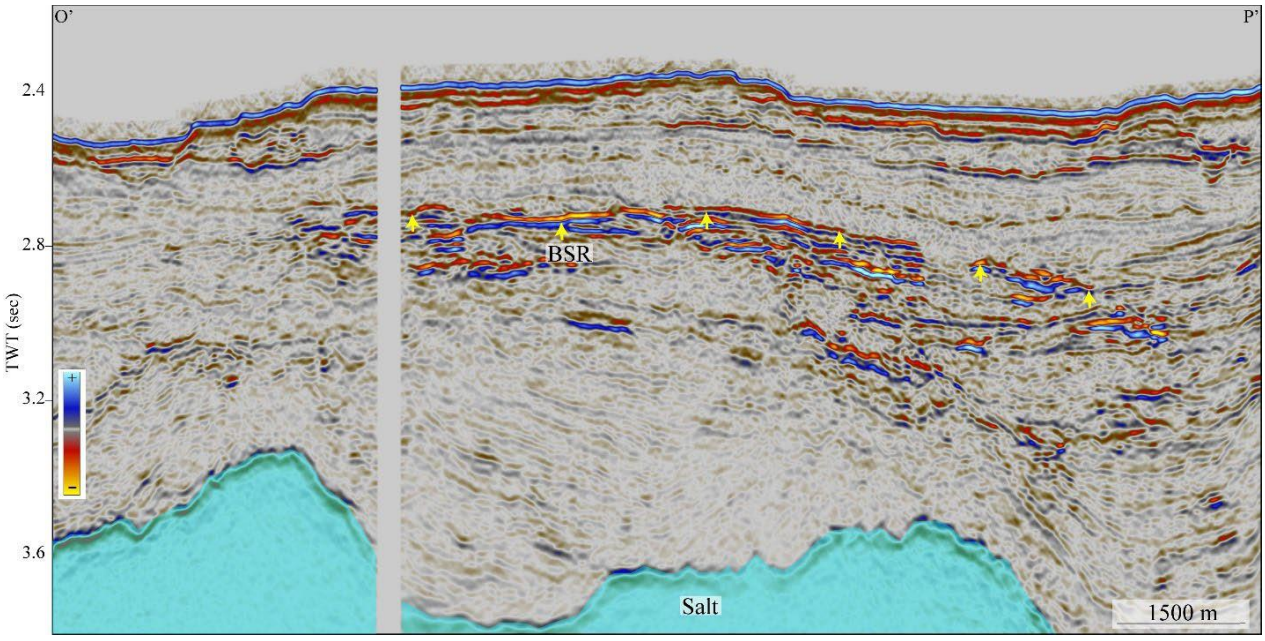

Figure 37: A seismic profile showing the south-north cross-section across the eastern BSR system of Zone-5. A clustered BSR is observed above the salt. The profile location is shown in Figure 36.

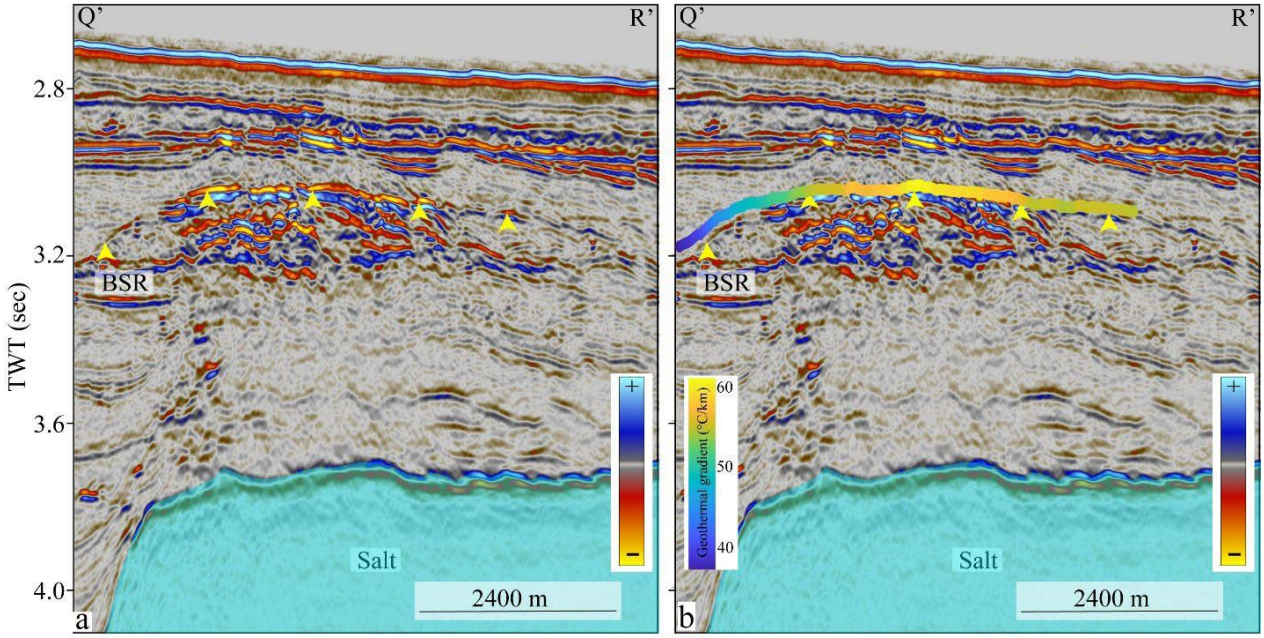

Figure 38: a) A seismic profile showing the northwest-southeast cross-section of the western BSR system of Zone-5. b) Geothermal gradient if overlaid over the seismic profile. A clustered BSR is observed above the salt. The profile location is shown in Figure 36.

5 Resource Estimation

The free gas volume at standard temperature and pressure V_g from hydrates at depth in the zone of peak-leading reflections is estimated using Equation 1.

$$V_g = 164At\phi S_h \text{.....Equation 1}$$

Where 164 is the volumetric conversion factor, A is the total area of peak-leading reflections in m^2, t is the sand thickness in m, ϕ is fraction of the bulk system that is the porosity, and S_h is the saturation of hydrate within that porosity. We calculate the minimum estimated resource by multiplying all of the minimum values together and the maximum resource by multiplying all of the maximum values together.

To estimate potential hydrate resources, we used the same range of values that we applied during the evaluation of Phase 1 Project Areas to peak leading reflections. This includes a minimum and maximum porosity of 30% and 40% a minimum and maximum sand thicknesses of 10 and 50 m, and minimum and maximum gas hydrate saturations of 50% and 90%. Below we explain each of the components of this formula in respect to the resource estimates provided in the current report.

1. Area (*A*)

We only perform resource calculations for the areas where we map peak-leading seismic responses above the BSR. This is because compressional (V_P) velocities exhibit sufficient changes only when hydrate concentration increases above ~40% (Yun, 2005). Due to velocity increase caused by medium to high saturation hydrate, there is an associated increase in the acoustic impedance which generates a peak leading response. A similar approach has been successfully used in several locations to map high-saturation hydrate in dipping sand layers (Frye et al., 2012; McConnell and Zhang, 2005; Portnov et al., 2022, 2021; Shedd et al., 2010). We do not calculate hydrate resource estimates for any other type of area.

2. Thickness of the sand layers (*t*)

Thickness is the most challenging component in absence of gamma ray logs. We use 10 m as a minimal estimate because this is roughly the thinnest bed that can be resolved given the average resolution of our

seismic data. We use an estimated maximum thickness of 50 m based on the multiple published well logs penetrating channel-levee systems in the Gulf of Mexico. The GC955 sand was more than 50 m thick, but only contained medium to high saturation hydrate in ~35 m (Collett et al., 2012). In the Ursa Basin, the thickness of low gamma ray, sand-rich units in IODP Expedition 308 wells (Ursa Basin, Gulf of Mexico) reaches 50 m (Sawyer et al (2009)).

3. Porosity (ϕ)

We use 30% as a minimum porosity and 40% as a maximum porosity based on a well-known depth-porosity function for a normally compacted coarse-grained sediment (i.e. the pore pressure is hydrostatic). We consider sediments up to 1 km below seafloor where 30 to 40% porosity are reasonable for lithology containing ~60-90% sand or coarse-silt (Cook and Sawyer, 2015; Kominz et al., 2011)

4. Hydrate Saturation (S_h)

As explained above, we provide resource estimates for potentially high-saturation accumulations. Peak-leading seismic responses may occur where hydrate saturations are above 40% (see #1 and (Yun, 2005)). We use 50% hydrate saturation for our minimum estimates. The highest estimate of 90% saturation is based on the drilled and depressurized hydrate cores in the GC955 Gulf of Mexico gas hydrate reservoir (e.g. Phillips et al (2020).

5. Volumetric conversion factor (164)

The volumetric conversion factor for gas hydrate can vary from 160 to 180, with a value of 164 (equating to an 85% occupation) being typically used (Boswell and Collett, 2011).

Given that 50% and 90% gas hydrate saturation should be confined to the areas with high-amplitude peak-leading amplitudes (~3 km^2), high-saturation gas hydrates in Project Area 2.4 may contain between 0.7 and 9 BCM of gas. The actual gas resources are likely significantly higher, since interpretation of peak-leading amplitudes highly depends on the data quality and signal frequency, which were not always favorable in Project Area 2.4.

6 Conclusions:

BSRs in Project Area 2.4 are associated with several buried channel systems and widespread salt tectonics. Underlying salt bodies create an anticlinal framework favorable for entrapment of gas at the base of gas hydrate stability and formation of multiple clustered BSRs that are good indicators of high-saturation gas hydrate reservoirs in turbidites (Portnov et al., 2019). Eight out of fourteen BSR zones in Project Area 2.4 show clustered BSRs above salt diapirs. We also observe hydrate systems are associated with faults and venting systems that likely supply the gas to the overlying hydrates systems.

Total BSR area in Project Area 2.4 is relatively very large (335 km^2) compared to the Project Areas 1-5 of Phase-I. The occurrence of peak-leading reflections (Zone-1 and Zone-2 BSR systems) and abundance of clustered BSRs in the Project Area 2.4 makes it a prospective area in terms of concentrated hydrate accumulation. However, lack of well data within many of the BSR systems prevents further in-depth analysis of the BSR systems identified. As more well data becomes available, a second look at Zone - 2, 3 and 5 could be warranted.

7 References:

Cook, A. E., & Sawyer, D. E. (2015). The mud-sand crossover on marine seismic data. *Geophysics, 80(6), A109–A114.* https://doi.org/10.1190/GEO2015-0291.1

Boswell, R., Collett, T.S. (2011). Current perspectives on gas hydrate resources. Energy Environ. Sci. https://doi.org/10.1039/c0ee00203h

Bureau of Ocean Energy Management (2022). Retrieved September 30, 2022, from https://www.boem.gov/oil-gas-energy/mapping-and-data/map-gallery

Collett, T. S., Lee, M. W., Zyrianova, M. V., Mrozewski, S. A., Guerin, G., Cook, A. E., & Goldberg, D. S. (2012). Gulf of Mexico Gas Hydrate Joint Industry Project Leg II logging-while-drilling data acquisition and analysis. *Marine and Petroleum Geology, 34*(1). https://doi.org/10.1016/j.marpetgeo.2011.08.003

Frye, M., Shedd, W., Boswell, R. (2012). Gas hydrate resource potential in the Terrebonne Basin, Northern Gulf of Mexico. Mar. Pet. Geol. 34, 150–168. https://doi.org/10.1016/j.marpetgeo.2011.08.001

Kominz, M.A., Patterson, K., Odette, D. (2011). Lithology dependence of porosity in slope and deep marine sediments. J. Sediment. Res. 81, 730–742. https://doi.org/10.2110/jsr.2011.60

Martinez, G. O., Sawyer, D. E., & Portnov, A. (2022). Seismic Geomorphology of the Chandeleur Submarine Landslide in the Northern Gulf of Mexico. *Geological Society, London, Special Publications*, *525*(1). https://doi.org/10.1144/sp525-2021-12

McConnell, D., Zhang, Z. (2005). Using acoustic inversion to image buried gas hydrate distribution. NETL-DOE Fire Ice 3–5.

Milkov, A. V, & Sassen, R. (2001). Estimate of gas hydrate resource, northwestern Gulf of Mexico continental slope. *Marine Geology*, *179*(1–2), 71–83. https://doi.org/10.1016/S0025-3227(01)00192-X

Phillips, S.C., Flemings, P.B., Holland, M.E., Schultheiss, P.J., Waite, W.F., Jang, J., Petrou, E.G., Hammon, H. (2020). High concentration methane hydrate in a silt reservoir from the deep-water Gulf of Mexico. Am. Assoc. Pet. Geol. Bull. 104, 1971–1995. https://doi.org/10.1306/01062018280

Portnov, A., Cook, A. E., Sawyer, D. E., Yang, C., Hillman, J. I. T., & Waite, W. F. (2019). Clustered BSRs: Evidence for gas hydrate-bearing turbidite complexes in folded regions, example from the Perdido Fold Belt, northern Gulf of Mexico. *Earth and Planetary Science Letters*, *528*, 115843. https://doi.org/10.1016/j.epsl.2019.115843

Portnov, A., Cook, A.E., Vadakkepuliyambatta, S. (2021). Diverse gas composition controls the Moby-Dick gas hydrate system in the Gulf of Mexico. Geology. https://doi.org/10.1130/G49310.1

Portnov, A., Cook, A.E., Sawyer, D.E. (2022). Bottom Simulating Reflections and Seismic Phase Reversals in the Gulf of Mexico. World Atlas Submar. Gas Hydrates Cont. Margins 315–322. https://doi.org/10.1007/978-3-030-81186-0_26

Shedd, W., Frye, M., Godfriaux, P., Dufrene, R., McConnell, D., Boswell, R., Collett, T., Mrozewski, S.,

Guerin, G., Cook, A., Shelander, D., Dai, J. (2010). Gulf of Mexico Gas Hydrates Joint Industry Project Leg II: Results from the Walker Ridge 313 Site. Offshore Technol. Conf. https://doi.org/10.4043/20806-MS

Shedd, W., Boswell, R., Frye, M., Godfriaux, P. & Kramer, K. (2012). Occurrence and nature of 'bottom simulating reflectors' in the northern Gulf of Mexico. *Marine and Petroleum Geology*, *34*(1), 31–40. https://doi.org/10.1016/j.marpetgeo.2011.08.005

Yun, T. S., Francisca, F. M., Santamarina, J. C., & Ruppel, C. (2005). Compressional and shear wave velocities in uncemented sediment containing gas hydrate. *Geophysical Research Letters*. https://doi.org/10.1029/2005GL022607